Available online at www.sciencedirect.com

ScienceDirect

Geochimica et Cosmochimica Acta 230 (2018) 60–82

Geochimica et Cosmochimica Acta

www.elsevier.com/locate/gca

Biogeochemical cycling of Mg and its isotopes in a sugar maple forest in Québec

Sara R. Kimmig [a,*], Chris Holmden [a], Nicolas Bélanger [b]

[a] *Saskatchewan Isotope Laboratory, Department of Geological Sciences, University of Saskatchewan, 114 Science Place, Saskatoon, SK S7N 5E2, Canada*

[b] *Département science et technologie, Université TÉLUQ, 5800, rue Saint-Denis, bureau 1105, Montréal, QC H2S 3L5, Canada*

Received 30 August 2017; accepted in revised form 25 March 2018; available online 5 April 2018

Abstract

A Mg isotope study of sugar maple (*Acer saccharum* Marsh.) in a field site in southern Québec, Canada, and seedlings grown in sterile soil substrate in the laboratory, both demonstrate per mil level within-tree Mg isotope fractionation. However, only sugar maple seedlings grown in the laboratory fractionate Mg isotopes during uptake into fine roots, favoring heavy isotope enrichment in the plant compared to the growth medium. Absence of uptake-related Mg isotope fractionation in field stands of sugar maple is tentatively attributed to the activities of the arbuscular mycorrhizal fungi that colonize fine roots of the trees in the field, but were absent from the laboratory grown specimens. The fungi facilitate nutrient uptake for the tree, while the tree provides valuable carbohydrates to the fungi. Without the symbiotic fungi, pot-grown trees in the laboratory are visibly stressed and often die. The mechanisms responsible for Mg isotopic fractionation in stressed trees remain to be elucidated. Rivers are isotopically light compared to bedrock weathering sources of Mg, and this has bearing on the δ^{26}Mg value of the continental weathering flux of Mg to the oceans, which is an important parameter in studies of ocean Mg cycling in the geological past. If uptake-related fractionation is negligible in many other naturally growing tree species, as it is in sugar maple, then forest growth will exert little or no influence on the δ^{26}Mg value of the export flux of Mg to first-order streams and rivers, and in turn the ocean Mg cycle. Above the tree line, preferential retention of heavy Mg isotopes in clay minerals formed during silicate weathering has been linked to the low δ^{26}Mg values in rivers. In the forested catchment of this study there is no clear evidence for these effects. The 1 N HNO_3 leach of the Bf-BC and C mineral soils, which are often used to identify minerals that may be releasing Mg and other base cations to plant-available pools, have the same average δ^{26}Mg value (−0.66‰, n = 2) as the litter layer and exchangeable leach of the forest floor, all soil solutions, and the stream (−0.63 ± 0.17‰ 2σ, n = 23). More revealing is the molar Mg/Ca ratio of the 1 N HNO_3 treatment (0.17), which is nearly identical to the bulk Mg/Ca ratio of the aboveground biomass (0.14). We conclude that the 1 N HNO_3 leach in this setting releases Mg from secondary minerals, such as vermiculite, other clays, and amorphous phases, which have taken up plant-recycled Mg and Ca that has filtered down through the soil from the litter layer of the forest floor. A single mineral, chlorite, with an estimated δ^{26}Mg value of −0.78‰, appears to be responsible for supplying most of the Mg that is circulating between the forest and soils in this setting, which is weathered and cached over timescales of thousands of years.

Keywords: Magnesium cycling; Magnesium isotopes; Biogeochemistry; Hardwood forest; Sugar maple; *Acer saccharum*; Arbuscular mycorrhizal fungi

* Corresponding author at: Biodiversity Institute, University of Kansas, Lawrence, KS 66045, USA.
E-mail address: srw039@mail.usask.ca (S.R. Kimmig).

https://doi.org/10.1016/j.gca.2018.03.020
0016-7037/

1. INTRODUCTION

Magnesium (Mg) is an essential macronutrient for plants, functioning as the coordinating cation of the chlorophyll molecule and as an enzyme activator for energy metabolism and synthesis of organic molecules. It is also required for the formation of RNA in the nucleus, aids in phosphate metabolism (ATP) and plant respiration and is integral to the maintenance of cellular pH and ionic balance (Wilkinson et al., 1990; Marschner, 1995; Epstein and Bloom, 2005; Barker and Pilbeam, 2007). Plant-available magnesium occupies ion exchange sites in soils (Wilkinson et al., 1990) where it is taken up by the fine roots of plants as an aqueous complex ($Mg(H_2O)_6^{2+}_{(aq)}$). Inside the plant, Mg exists in both the free ion and chelated forms and is translocated when needed from older plant tissues to younger growing leaves, seeds, and roots (Wilkinson et al., 1990; Marschner, 1995; Barker and Pilbeam, 2007; Black et al., 2008). Plant rooting activity and organic matter oxidation in soils generates carbonic acid, which accelerates mineral weathering (Drever, 1994; Berner, 1997; Walker et al., 2003; Derry et al., 2005). At the local scale, mineral weathering provides vital nutrients for vegetative growth. At the global scale, continental weathering of Ca- and Mg-bearing silicate minerals regulates atmospheric CO_2 and climate on million-year timescales (Eq. (1)) (Berner et al., 1983).

$$CO_2 + (Ca, Mg)SiO_3 \rightarrow (Ca, Mg)CO_3 + SiO_2 \quad (1)$$

Field and laboratory studies demonstrate that plants (Black et al., 2008; Bolou-Bi et al., 2010, 2012; Tipper et al., 2010, 2012b; Opfergelt et al., 2014; Mavromatis et al., 2014; Uhlig et al., 2017) and fungi (Fahad et al., 2016; Pokharel et al., 2017) fractionate Mg isotopes, as documented by differences in $\delta^{26}Mg$ values between Mg nutritive solutions and plants, and between different tissues of plants, such as roots, shoots, leaves, and seeds (Table S1). Some of this Mg is recycled back into the plant through litter degradation, and some is lost to groundwater, streams, and rivers. Magnesium isotopes can be used to trace elemental Mg cycling in Earth surface environments. A question of importance in Mg isotope research relates to the $\delta^{26}Mg$ value of the continental weathering flux of Mg to the oceans on a global scale, is it a reflection of mineral weathering processes or plant-cycling processes?

Mineral weathering processes have been investigated in sparsely vegetated environments, such as the Himalaya and Tibetan Plateau, where Tipper et al. (2006a, 2008) found streams and rivers draining silicate dominated watersheds with lower $\delta^{26}Mg$ (–1.25‰) than local bedrock values (−0.48‰). They attributed this effect to the preferential retention of heavy Mg isotopes in clay minerals formed during silicate weathering. Wimpenny et al. (2011) reported a similar effect in non-glacial rivers in Greenland (−0.63‰) draining lightly vegetated silicate bedrock (−0.42‰). However, these authors considered trace calcite weathering as an additional factor contributing to the low $\delta^{26}Mg$ values of rivers (cf., Jacobson et al., 2002; Moore et al., 2013; Jacobson et al. 2015). Calcite dissolves more easily than silicates and is lower in $\delta^{26}Mg$ value, ranging between −1.1 and −5.2‰ (Li et al., 2012; Saenger and Wang, 2014). Calcite may also be found as trace inclusions in silicate minerals (Ryu et al., 2011; Ryu et al., 2016), which makes it difficult to neglect calcite weathering even in settings where there is no bedded marine carbonate (Blum et al., 1998; White et al., 1999; Jacobson and Blum, 2000). A number of other studies have reported rivers with low $\delta^{26}Mg$ values in catchments underlain by silicate bedrock with the effect generally attributed to the retention of heavy Mg isotopes by clays and amorphous phases formed during silicate weathering (Tipper et al., 2006b, 2010, 2012a, b; Brenot et al., 2008; Pogge von Strandmann et al., 2012; Teng et al., 2010; Opfergelt et al., 2012, 2014; Huang et al., 2012; Liu et al., 2014; Mavromatis et al., 2014; Dessert et al., 2015; Ma et al., 2015; Chapela Lara et al., 2017), although there are some reported instances of clay formation favoring the uptake of light Mg isotopes (Pogge von Strandmann et al., 2008; Wimpenny et al., 2010; Li et al., 2014), which would be expected to drive environmental waters to higher $\delta^{26}Mg$ values. A survey of the literature shows that rivers identified as draining silicate dominated watersheds are on average $\sim -0.42 \pm 0.17$‰ (2s.e., n = 14) lower than the local silicate bedrock (Table S2).

Biogeochemical cycling of Mg between vegetation and soils could potentially be another source of light Mg isotopes to rivers. Black et al. (2008) showed that hydroponically grown wheat preferentially sequesters heavy Mg isotopes, driving nutrient solutions to lower $\delta^{26}Mg$ values with an apparent fractionation factor ($\Delta^{26}Mg_{plant\text{-}source}$) of ~+0.20‰. Bolou-Bi et al. (2010) showed that hydroponically grown clover is 0.41‰ higher in $\delta^{26}Mg$ than its nutrient solution. These studies have been influential in cultivating the idea that trees favor the uptake of heavy Mg isotopes from soil solutions, thus driving streams and rivers to lower $\delta^{26}Mg$ values (Tipper et al., 2010; Bolou-Bi et al., 2012). However, the evidence detailing this effect in the field is more difficult to acquire and interpret than in the laboratory. For example, there is a wide range of within-plant Mg isotope fractionations among different tree tissues, such as roots, stems, and leaves, that make it difficult to determine the $\delta^{26}Mg$ value of the vegetation as a whole. A similar problem hampers identification of nutrient Mg sources in soils, and there is the additional consideration of the undefined role played by mycorrhizal fungi in the capture of nutrients by tree fine roots (Smith and Read, 2008). In cases where whole plant data have been presented, or where stemwood is considered to be the largest and potentially least fractionated pool of Mg in trees, a review of the literature yields an average $\Delta^{26}Mg$ value of $+0.14 \pm 0.16$‰ (2s.e.) (Table S1) for the apparent uptake-related fractionation factor. The positive fractionation is consistent with the premise that Mg cycling in forests can induce the preferential export of light Mg isotopes to streams and rivers, but the effect is smaller than a similar search of the literature for the average fractionation associated with laboratory grown plants ($+0.59 \pm 0.39$, 2 s.e., n = 5) (Table S1).

In this paper, Mg isotope fractionation in sugar maple (*Acer saccharum* Marsh.), an emblematic tree species in Canada, is investigated in the field and laboratory. The

aim of this study is to determine the impact of forest Mg cycling on the export signature of Mg isotopes to a first-order stream. Measurements of δ^{26}Mg values in fine roots, stemwood, xylem exudates (sap), foliage (senescent and photosynthesizing), and litterfall from a mature sugar maple tree and seedlings are presented, as well as soil (solid and liquid phases), rock, throughfall, bulk precipitation, lake water, and stream water. In addition, sugar maple seedlings were cultivated in the laboratory to help distinguish uptake-related Mg isotope fractionation in tree fine roots from within-tree sources of fractionation, as well as the complicated processes controlling Mg source and availability in soils.

2. STUDY SITE AND SAMPLING METHODS

2.1. Study site description

The field study was conducted in the Hermine Experimental Watershed (HEW), a first-order, spring-fed catchment located within an unmanaged northern hardwood forest of the *Station de Biologie des Laurentides* (SBL) of *Université de Montréal*, approximately 80 km north of Montréal, Québec, Canada, near the town of Saint-Hippolyte in the Lower Laurentians (Fig. 1). The forest has a mean basal area of approximately 29 m^2 ha^{-1} with a mean overstory age of ~90 years and heights ranging from 20 to 25 m (Courchesne et al., 2005). The present-day forest is the result of secondary succession following a fire disturbance in the 1920s (Bélanger et al., 2004). Mean July and December air temperatures are 19 °C and −10 °C, respectively, with a mean annual precipitation of 1100 mm, 30% of which falls as snow. Overstory vegetation is ~65% sugar maple, with subsidiary populations of American beech (*Fagus grandifolia* Ehrh.), red maple (*Acer rubrum* L.), yellow birch (*Betula alleghaniensis* Britt.), paper birch (*Betula papyrifera* Marsh.), balsam fir (*Abies balsamea* (L.) Mill.), and bigtooth aspen (*Populus grandidentata* Michx.) (Liu and Côté, 1993; Vizcayno-Soto and Côté, 2004; Bélanger et al., 2004). Understory vegetation consists primarily of striped maple (*Acer pennsylvanica* L.), hobblebush (*Viburnum lantanoides* Michx.), wood fern (*Dryopteris* sp.), and lycopods (*Lycopodium* sp.).

The bedrock of the watershed is anorthosite belonging to the Morin anorthosite-charnockite complex within the Grenville Province with ages between 1165 Ma and 1135 Ma (Doig, 1991; Friedman and Martignole, 1995). The study site is situated approximately five kilometers west of an anorthosite-orthopyroxene granitoid contact zone and southeast of a series of granitic gneisses, charnockite gneiss, orthopyroxene bearing granitoids, and marble (Martignole and Schrijver, 1970; Emslie, 1975). During the last glaciation, ice sheets covered the landscape, advancing from the northwest. The forests are developed on allochthonous glacial till, with a mineralogical makeup and chemical composition differing greatly from the underlying anorthosite bedrock (e.g., Bélanger et al., 2012), which outcrops in a few areas within the watershed. The soils are fairly thin (< 2 m to the bedrock) and consist mostly of Orthic Humo-Ferric Podzols (SCWG, 1998). The dominant Mg-containing minerals in the soil are chlorite, vermiculite, and biotite. These are not primary mineral constituents of the anorthosite, and so must be predominantly contributed by the parent till.

A permanent plot was established in the HEW in the summer of 2010 located at 45.984°N and 074.014°W, 387 ± 11 m. The overstory vegetation consists predominantly of sugar maple (Figs. 1 and 2).

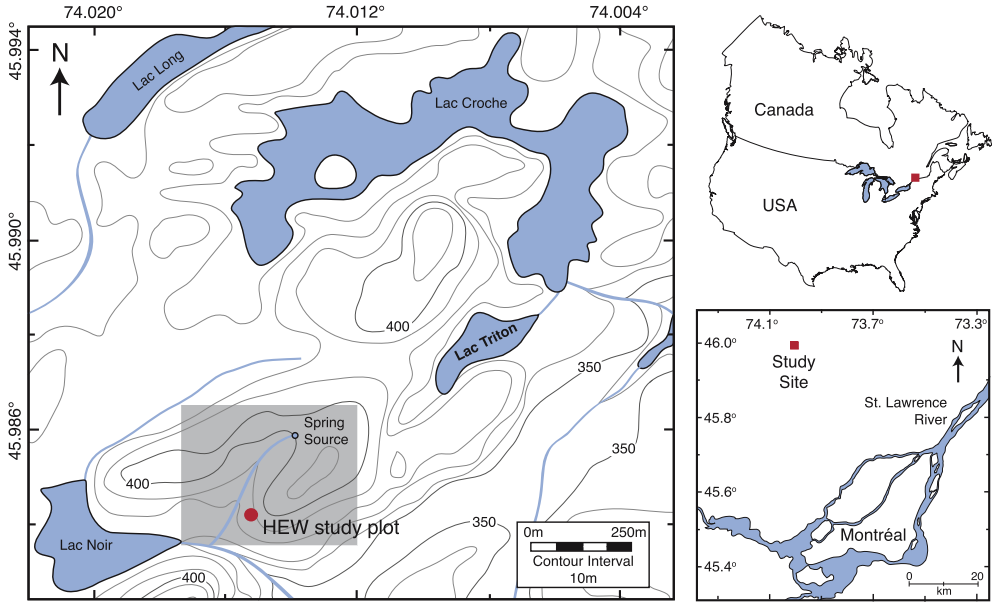

Fig. 1. Maps showing the North American location of the HEW study site, approximately 80 km north of the city of Montréal, Québec, Canada. The boundaries of the HEW are depicted by the shaded grey area on the topographic map. The red circle is the location of the study plot. (For interpretation of the references to colour in this figure legend, the reader is referred to the web version of this article.)

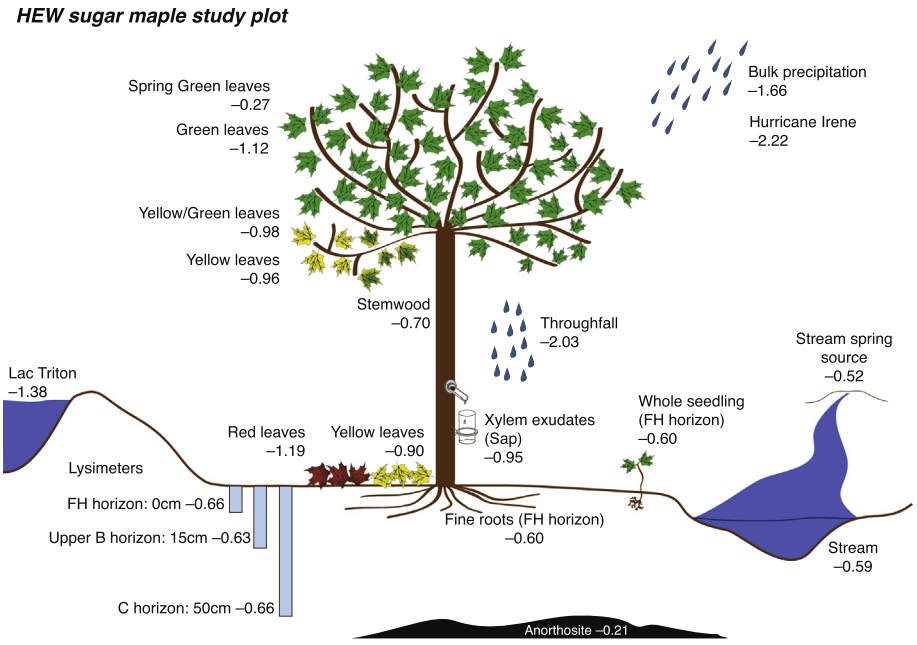

Fig. 2. δ^{26}Mg values for various components of the Mg cycle in the HEW field site. Note that some foliage was collected live from the tree, and some leaves (red and yellow) were collected on the forest floor during autumnal senescence. (For interpretation of the references to color in this figure legend, the reader is referred to the web version of this article.)

2.2. Sample collection

Zero-tension 'nested' lysimeters were installed in the study plot in June 2010 following the protocols detailed in MacDonald et al. (2007) at depths corresponding to directly below the forest floor (0 cm), the upper B horizon (15 cm), and C horizon (50 cm), which is below the rooting zone. The lysimeters were left to equilibrate with soil solutions over several months during which time they were purged of water. The lysimeters were sampled for this study in October 2010, May 2011, and October 2012 using trace metal clean high-density polyethylene (HDPE) bottles. Soils were sampled during the installation of the lysimeters, and visually confirmed to be an Orthic Humo-Ferric Podzol consisting of five soil horizons in the following sequence: FH, Ae, Bhf (thin), Bf-BC, and C. The forest floor (FH horizon), lower podzolic (Bf-BC horizon), and mineral soil (C horizon) were sampled for Mg isotope study. A piece of exposed anorthosite bedrock was also sampled.

Groundwater was collected in autumn of 2009 from the spring source of the stream using trace metal clean HDPE bottles. Stream waters were collected just upstream from the study plot in July and August of 2010, during low and high (following a rain event) flows in September 2010, and again in June of the following year. In addition, water from Lac Triton, a small lake located ~0.5 km from the study plot with a surface area of ~0.02 km^2 and a shallow depth of 3.7 m (Fig. 1), was also sampled at low and high water levels. Rainwater was collected as bulk (wet and dry) deposition between July and September 2010 using a funnel that was attached with Tygon tubing to a sample bottle housed within a cooler. The funnel collection system was fixed to a tower at a height of 20 m to limit contamination from the canopy. The tower is located 500 m outside of the HEW. The sample bottles in the cooler were completely covered, except for the funnel inlet, in order to reduce evaporation of the samples prior to retrieval. Samples were collected in 1 L trace metal clean low density polyethylene (LDPE) bottles, filtered with 0.45 μm polycarbonate membranes, and acidified to a pH of ~0.7 with the addition of ultrapure 15 N HNO_3. In August of 2011, hurricane Irene passed through the field site and was sampled as a separate event. Throughfall samples were collected in September of 2010 using temporary collectors in two locations within the study plot. The collectors consisted of funnels attached with Tygon tubing to HDPE bottles on the ground. A plug of trace metal clean fibrous polyester was used in the neck of the funnel collector to block particulate matter from entering the collection bottle. Funnels, bottles, and Tygon tubing for the collectors were acid cleaned in the laboratory prior to installation.

Sugar maple vegetation samples (foliage, stemwood, fine roots) were collected from the same tree, identified as 'Sugar Maple 3' (SM3) (Table 1). Diameter at breast height (DBH) (~1.3 m from the ground) was 10.2 cm. Foliage from SM3 located in the upper half of the canopy was sampled in September of 2010 with a telescopic pole pruner prior to and during various stages of leaf senescence, as well as from the following year's spring canopy. Foliage samples were collected throughout the senescent period and categorized by color, including (1) green leaves, (2) yellow/green leaves, and (3) yellow leaves. Stemwood was sampled using a Haglöf increment borer in September of 2010 at ~1.3 m above the ground. The wood cores were stored in the field in plastic drinking straws prior to being transported back to the lab for processing. Fine roots (<2 mm diameter) were sampled at the base of SM3 from the forest floor (FH hori-

Table 1
Detailed Mg isotope data, Ca, Mg, and Sr concentrations as well as Sr/Ca and Mg/Ca molar ratios for precipitation, throughfall, stream water, lake water, soil solutions, plant tissues (foliage, wood, roots, seedlings, understory), xylem exudates (saps), soil and rock extracts/digests at the HEW study plot. Magnesium duplicates refer to sample solutions duplicated through chemical separation and analysis. Prepared Mg solutions that were analyzed in separately tuned mass spectrometry sessions are shown with 2 standard deviations (2σ) error. Those analyzed within the same tuned sessions are denoted by 2 standard errors of the mean (2s.e.).

Sample ID	Sample type	Sample description	N	δ^{26}Mg (‰DSM3)	2 s.e.	2σ	δ^{25}Mg (‰DSM3)	2 s.e.	2σ	Δ^{25}Mg' [a]	Ca (ppm)	Mg (ppm)	Sr (ppm)	Fe (ppm)	Ca/Mg (mol/mol)	Mg/Ca (mol/mol)	Sr/Mg (mmol/mol)	Sr/Ca (mmol/mol)	Fe/Mg (mol/mol)
Bulk precipitation																			
W18	Rain water	July Bulk	2	−1.73		0.04	−0.90		0.03	0.00	0.236	0.043	0.001		3.33	0.300	3.50	1.05	
W23	Rain water	August/September Bulk	4	−1.58	0.02		−0.82	0.02		0.00	0.450	0.071	0.001		3.85	0.259	4.27	1.11	
		average	*2*	*−1.66*		*0.21*	*−0.86*		*0.12*		*0.343*	*0.057*	*0.001*		*3.59*	*0.278*	*3.89*	*1.08*	
Hurricane Irene																			
W34	Event rain	Bulk precipitation 2011	2	−2.22		0.15	−1.13		0.06	0.02	0.176	0.041	0.000		2.64	0.379	2.40	0.91	
Throughfall																			
W09	Throughfall	Collector 2	2	−2.76		0.06	−1.42		0.03	0.02	0.703	0.073	0.003		5.86	0.171	10.8	1.83	
W10	Throughfall	Collector 1	4	−1.30	0.02		−0.68	0.01		−0.01	0.475	0.059	0.002		4.86	0.206	8.19	1.69	
		average	*2*	*−2.03*		*2.07*	*−1.05*		*1.04*		*0.589*	*0.066*	*0.002*		*5.36*	*0.188*	*9.47*	*1.76*	
Lake water																			
W07	Lake water	Lac Triton – High Level	4	−1.13	0.02		−0.59	0.01		−0.01	2.23	0.448	0.015		3.02	0.331	9.40	3.11	
W33	Lake water	Lac Triton – Low Level	4	−1.64	0.06		−0.86	0.02		−0.01	1.84	0.308	0.012		3.62	0.276	10.9	3.00	
		average	*2*	*−1.38*		*0.73*	*−0.73*		*0.38*		*2.03*	*0.38*	*0.014*		*3.32*	*0.301*	*10.1*	*3.05*	
Groundwater																			
KETTLE	Groundwater	Spring Source 2009	4	−0.52	0.04		−0.26	0.02		0.01	2.49	0.230	0.020		6.57	0.152	24.5	3.73	
Stream water																			
W05	Stream water	Low Flow September	4	−0.60	0.03		−0.31	0.03		0.01	2.70	0.463	0.018		3.53	0.283	10.8	3.06	
W06	Stream water	High Flow September	4	−0.77	0.04		−0.40	0.02		0.00	2.33	0.370	0.016		3.82	0.261	12.4	3.23	
W16	Stream water	July Bulk	3	−0.57	0.04		−0.30	0.01		0.00	2.14	0.351	0.015		3.71	0.270	11.6	3.14	
W20	Stream water	August Bulk	4	−0.51	0.01		−0.27	0.02		0.00	2.56	0.328	0.018		4.74	0.211	14.8	3.13	
W22	Stream water	August/Sept Bulk	4	−0.43	0.05		−0.21	0.03		0.01	2.07	0.362	0.013		3.48	0.288	10.3	2.98	
W24	Stream water	Low Flow June 2011	4	−0.58	0.01		−0.30	0.02		0.01	2.03	0.320	0.015		3.85	0.260	12.6	3.27	
W30	Stream water	Low Flow June 2011	3	−0.72	0.02		−0.40	0.02		−0.02	2.13	0.345	0.015		3.75	0.266	12.2	3.24	
		average	*7*	*−0.60*		*0.23*	*−0.31*		*0.13*		*2.28*	*0.362*	*0.016*		*3.84*	*0.260*	*12.1*	*3.15*	
Soil solutions																			
W11	Lysimeter	0 cm – Autumn 2010	4	−0.73	0.03		−0.38	0.02		0.00	6.64	0.571	0.050		7.06	0.142	24.3	3.44	
W11d	Lysimeter	0 cm – Mg duplicate	3	−0.64	0.01		−0.33	0.02		0.01									
W25	Lysimeter	0 cm – Spring 2011	4	−0.59	0.04		−0.31	0.02		0.00	4.50	0.398	0.033		6.86	0.146	23.0	3.34	
W31	Lysimeter	0 cm – Spring 2011	4	−0.63	0.04		−0.33	0.01		0.00	3.88	0.305	0.025		7.73	0.129	23.2	3.00	
W36	Lysimeter	0 cm – Autumn 2012	3	−0.61	0.04		−0.31	0.01		0.00	4.32	0.327	0.036		8.01	0.125	30.2	3.77	
W39	Lysimeter	0 cm – Autumn 2012	4	−0.75	0.03		−0.38	0.05		0.01	4.24	0.304	0.035		8.46	0.118	32.3	3.82	
W12	Lysimeter	15 cm – Autumn 2010	3	−0.69	0.06		−0.35	0.03		0.01	4.32	0.597	0.036		4.39	0.228	16.5	3.77	
W12d	Lysimeter	15 cm – Mg duplicate	3	−0.65	0.05		−0.33	0.03		0.01									
W26	Lysimeter	15 cm – Spring 2011	4	−0.66	0.05		−0.32	0.01		0.02	3.59	0.525	0.030		4.14	0.241	16.0	3.86	
W40	Lysimeter	15 cm – Autumn 2012	4	−0.52	0.07		−0.26	0.06		0.01	4.45	0.583	0.038		4.63	0.216	18.1	3.91	
W13	Lysimeter	50 cm – Autumn 2010	4	−0.72	0.02		−0.38	0.02		−0.01	1.79	0.255	0.016		4.24	0.236	17.1	4.03	
W27	Lysimeter	50 cm – Spring 2011	4	−0.72	0.02		−0.36	0.01		0.01	1.77	0.307	0.015		3.50	0.286	13.6	3.89	
W32	Lysimeter	50 cm – Spring 2011	4	−0.68	0.05		−0.36	0.03		0.00	2.18	0.306	0.017		4.32	0.231	15.1	3.50	
W41	Lysimeter	50 cm – Autumn 2012	3	−0.51	0.09		−0.28	0.03		−0.01	2.19	0.245	0.018		5.42	0.184	20.3	3.74	
		average	*14*	*−0.65*		*0.15*	*−0.33*		*0.07*		*3.66*	*0.394*	*0.029*		*5.73*	*0.175*	*20.8*	*3.67*	
Fine roots																			
V25	Sugar maple 3	June 2010	1	−0.48			−0.23			0.02	11,014	1341	115		4.98	0.201	23.8	4.78	
V49	Sugar maple 3	September 2010	4	−0.72	0.02		−0.37	0.01		0.01	5411	688	53.6		4.77	0.210	21.6	4.53	
		average	*2*	*−0.60*		*0.34*	*−0.30*		*0.20*		*8213*	*1015*	*84.4*		*4.87*	0.205	*22.7*	*4.66*	

Stemwood																		
V42	Sugar maple 3	Core 1	3	−0.76	0.06		−0.43	0.02		−0.03	2739	115	25.1		14.5	0.069	60.8	4.20	
V43	Sugar maple 3	Core 2	2	−0.63		0.01	−0.31		0.02	0.01	3477	233	28.7		9.07	0.110	34.2	3.77	
		average	*2*	*−0.70*		*0.19*	*−0.37*		*0.17*		*3108*	*174*	*26.9*		*11.8*	*0.085*	*47.5*	*3.99*	
Autumn foliage																			
V51	Sugar maple 3	Green Leaves	3	−1.19	0.03		−0.60	0.03		0.02	16,715	1641	120		6.18	0.162	20.2	3.27	
V51−2	Sugar maple 3	Green Leaves	4	−1.05	0.03		−0.54	0.02		0.01	16,322	1585	108		6.24	0.160	19.0	3.04	
V52	Sugar maple 3	Yellow/Green Leaves	4	−1.10	0.07		−0.56	0.04		0.01	12,533	853	91.0		8.92	0.112	29.6	3.32	
V52−2	Sugar maple 3	Yellow/Green Leaves	4	−0.86	0.05		−0.45	0.03		0.00	12,584	1396	90.0		5.47	0.183	17.9	3.27	
V53	Sugar maple 3	Yellow Leaves	3	−0.88	0.05		−0.46	0.04		0.00	17,278	1416	124		7.40	0.135	24.2	3.28	
V53−2	Sugar maple 3	Yellow Leaves	4	−1.03	0.03		−0.54	0.02		0.00	17,820	1740	121		6.21	0.161	19.3	3.11	
		average	*6*	*−1.02*		*0.25*	*−0.53*		*0.12*		*15,542*	*1439*	*109*		*6.74*	*0.148*	*21.7*	*3.22*	
Leaf litter																			
V33	Sugar maple	Red Leaves	4	−1.32	0.06		−0.66	0.04		0.02	12,335	1150	81.2		6.51	0.154	19.6	3.01	
V33-2	Sugar maple	Red Leaves	3	−1.06	0.11	0.11	−0.54	0.07	0.07	0.01	13,822	1027	82.0		8.16	0.123	22.2	2.71	
V34	Sugar maple	Yellow Leaves	4	−0.90	0.01		−0.47	0.01		0.00	9824	970	66.6		6.14	0.163	19.1	3.10	
		average	*3*	*−1.09*		*0.42*	*−0.56*		*0.19*		*11,994*	*1049*	*76.6*		*6.94*	*0.144*	*20.3*	*2.94*	
Spring foliage																			
V55	Sugar maple 3	Spring Green Leaves	4	−0.13	0.06		−0.06	0.03		0.01	4142	1333	25.8		1.88	0.531	5.36	2.84	
V55-2	Sugar maple 3	Spring Green Leaves	4	−0.40	0.02		−0.20	0.02		0.00	4006	1273	25.7		1.91	0.524	5.60	2.94	
		average	*2*	*−0.27*		*0.37*	*−0.13*		*0.20*		*4074*	*1303*	*25.7*		*1.90*	*0.527*	*5.5*	*2.89*	
Seedlings																			
V35	Sugar maple	Autumn Seedling (whole)	4	−0.60	0.02		−0.30	0.02		0.01	6341	919	54.2		4.18	0.239	16.4	3.91	
V35r-1	Sugar maple	Autumn Seedling Root	4	−0.47	0.01		−0.25	0.03		−0.01	9798	695	89.2		8.55	0.117	35.6	4.16	
V35s-1	Sugar maple	Autumn Seedling Stem	4	−0.64	0.04		−0.33	0.04		0.00	2415	609	28.7		2.40	0.416	13.1	5.44	
V35l-1	Sugar maple	Autumn Seedling Leaves	4	−0.74	0.03		−0.38	0.02		0.01	12,816	1970	75.5		3.95	0.253	10.6	2.69	
V35-1		Whole (calculated)		−0.66			−0.34												
V35r-2	Sugar maple	Autumn Seedling Root	4	−0.35	0.02		−0.19	0.02		−0.01	6348	507	61.0		7.59	0.132	33.4	4.40	
V35s-2	Sugar maple	Autumn Seedling Stem	4	−0.78	0.05		−0.40	0.04		0.01	2772	564	31.0		2.98	0.336	15.2	5.12	
V35l-2	Sugar maple	Autumn Seedling Leaves	4	−0.82	0.04		−0.42	0.02		0.01	11,592	1732	82.3		4.06	0.246	13.2	3.25	
V35-2		Whole (calculated)		−0.73			−0.37												
		average (whole)	*3*	*−0.66*		*0.13*	*−0.34*		*0.07*										
Xylem exudates (saps)																			
SBL01	Early season	1.5°Bx sugar content	4	−0.79	0.06		−0.41	0.03		0.00	2180	253	15.0		5.23	0.191	16.4	3.14	
SBL01	Mid season	3.4°Bx sugar content	4	−0.99	0.03		−0.54	0.01		−0.02	1144	174	8.12		4.00	0.250	13.0	3.25	
SBL01	Late season	3.3°Bx sugar content	4	−0.80	0.03		−0.42	0.01		−0.01	1694	243	10.8		4.23	0.236	12.3	2.91	
SBL02	Early season	1.8°Bx sugar content	4	−0.89	0.04		−0.46	0.01		0.01	2119	259	13.8		4.96	0.202	14.8	2.98	
SBL02	Mid season	4.4°Bx sugar content	4	−1.02	0.04		−0.53	0.03		0.00	1821	222	11.7		4.98	0.201	14.6	2.93	
SBL02	Late season	2.1°Bx sugar content	4	−1.03	0.05		−0.54	0.02		0.00	2173	272	15.0		4.85	0.206	15.3	3.15	
SBL03	Early season	1.7°Bx sugar content	4	−1.07	0.03		−0.55	0.03		0.01	1580	191	10.9		5.01	0.200	15.8	3.15	
SBL03	Mid season	2.1°Bx sugar content	4	−0.83	0.02		−0.44	0.04		−0.01	3005	348	19.5		5.24	0.191	15.6	2.97	
SBL03	Late season	2.1°Bx sugar content	4	−0.86	0.10		−0.44	0.04		0.00	3633	431	23.6		5.12	0.195	15.2	2.98	
SBL04	Mid season	2.4°Bx sugar content	4	−1.10	0.01		−0.57	0.01		0.00	2722	279	17.0		5.92	0.169	16.9	2.85	
SBL04	Late season	1.5°Bx sugar content	4	−1.10	0.03		−0.55	0.02		0.02	3234	349	20.8		5.62	0.178	16.5	2.94	
		average	*11*	*−0.95*		*0.24*	*−0.50*		*0.12*		*2300*	*274*	*15.1*		*5.02*	*0.199*	*15.1*	*3.02*	
Soil extracts – Forest floor (FH Horizon)																			
S06	FH	Bulk Digest	4	−0.64	0.07		−0.32	0.04		0.02	8363	917	71.1	5246	5.53	0.181	21.5	3.89	2.49
S06	FH	0.1 N $BaCl_2$ Leach	4	−0.59	0.02		−0.29	0.03		0.02	2841	103	35.2	9.47	16.6	0.060	94.4	5.67	0.040
S06	FH	0.1 N HCl Leach	4	−0.74	0.07		−0.37	0.04		0.01	977	38.4	4.02	128	15.4	0.065	29.0	1.88	1.45
S06	FH	1 N HNO_3 Leach	4	−0.30	0.02		−0.10	0.04		0.06	284	11.3	2.81	544	15.3	0.065	69.4	4.53	21.0
S06	FH	15 N HNO_3 Leach	4	−0.43	0.01		−0.21	0.02		0.02	204	74.8	2.27	2259	1.65	0.605	8.41	5.09	13.1
S06	FH	Residue Digest	4	−0.37	0.02		−0.18	0.02		0.02	4761	2129	89.1	9388	1.36	0.737	11.6	8.56	1.92

(*continued on next page*)

Table 1 (*continued*)

Sample ID	Sample type	Sample description	N	δ^{26}Mg (‰DSM3)	2 s.e.	2σ	δ^{25}Mg (‰DSM3)	2 s.e.	2σ	Δ^{25}Mg* [a]	Ca (ppm)	Mg (ppm)	Sr (ppm)	Fe (ppm)	Ca/Mg (mol/mol)	Mg/Ca (mol/mol)	Sr/Mg (mmol/mol)	Sr/Ca (mmol/mol)	Fe/Mg (mol/mol)
Soil extracts – Bf-BC Horizon																			
S10	Bf-BC	Bulk Digest	4	−0.75	0.06		−0.36	0.05		0.03	18,572	6663	212	27,159	1.69	0.592	8.84	5.23	1.77
S10	Bf-BC	0.1 N $BaCl_2$ Leach	2	−1.65	0.09		−0.83	0.00		0.03	20.2	0.77	8.39	0.578	15.9	0.063	3022	190	0.326
S10	Bf-BC	0.1 N HCl Leach									473	1.14	1.10	20.2	252	0.004	269	1.07	7.72
S10	Bf-BC	1 N HNO_3 Leach	4	−0.66	0.03		−0.32	0.02		0.02	249	24.7	0.462	816	6.12	0.164	5.18	0.848	14.4
S10	Bf-BC	15 N HNO_3 Leach	4	−0.08	0.03		−0.03	0.02		0.02	168	1270	0.995	4905	0.080	12.4	0.22	2.70	1.68
S10	Bf-BC	Residue Digest	4	−0.69	0.03		−0.33	0.02		0.02	16,505	6341	198	24,426	1.58	0.634	8.65	5.48	1.68
Soil extracts – C Horizon																			
S11	C	Bulk Digest	4	−0.71	0.04		−0.34	0.02		0.03	23,963	8032	220	31,558	1.81	0.553	7.58	4.19	1.71
S11	C	0.1 N $BaCl_2$ Leach	3	−2.07	0.04		−1.03	0.05		0.05	25.7	1.03	11.0	0.618	15.2	0.066	2957	195	0.261
S11	C	0.1 N HCl Leach	3	−0.80	0.09		−0.40	0.07		0.01	719	1.84	1.37	47.5	237	0.004	206	0.872	11.2
S11	C	1 N HNO_3 Leach	4	−0.66	0.02		−0.31	0.02		0.03	309	31.9	0.573	473	5.89	0.170	4.98	0.847	6.46
S11	C	15 N HNO_3 Leach	4	−0.05	0.04		−0.03	0.01		−0.01	235	1533	1.47	5455	0.093	10.7	0.266	2.86	1.55
S11d	C	15 N HNO_3 – Mg duplicate	3	−0.01	0.07		−0.02	0.05		−0.02									
S11	C	Residue Digest	4	−0.65	0.01		−0.30	0.01		0.03	21,496	7163	222	26,375	1.82	0.549	8.60	4.72	1.60
Bedrock extracts																			
R01	Anorthosite	Bulk Digest	4	−0.21	0.08		−0.10	0.04		0.01	78,965	13,470	650	17,939	3.56	0.281	13.4	3.77	0.580
R01-2	Anorthosite	Bulk – Duplicate digest	3	−0.21	0.04		−0.11	0.05		0.00	80,977	13,704	623	17,837	3.58	0.279	12.6	3.52	0.566
R01	Anorthosite	0.1 N $BaCl_2$ Leach	4	−1.10	0.04		−0.58	0.01		−0.01	233	12.4	12.1		11.4	0.088	271	23.7	
R01	Anorthosite	0.1 N HCl Leach	3	−0.15	0.03		−0.08	0.00		0.00	1372	167	4.90	284	4.97	0.201	8.11	1.63	0.737
R01	Anorthosite	1 N HNO_3 Leach	4	−0.32	0.03		−0.17	0.02		0.00	607	177	4.11	284	2.08	0.480	6.45	3.10	0.700
R01	Anorthosite	15 N HNO_3 Leach	4	−0.26	0.03		−0.13	0.05		0.00	7484	2321	51.7	3242	1.96	0.511	6.18	3.16	0.608
R01d	Anorthosite	15 N HNO_3 - Mg duplicate	4	−0.22	0.02		−0.11	0.02		0.01									

[a] Calculated using methods from Young and Galy (2004).

zon). Fine root samples were taken in June of 2010 during the installation of the nested lysimeters, and again in September of 2010, by sampling a shallow pit dug at the base of the studied tree.

Leaf litterfall was collected in September of 2010. Only pristine sugar maple leaves without any evidence of decomposition were chosen for sampling. Throughout leaf senescence, litterfall was categorized by color, denoted as yellow and red leaves (Fig. 2). Yellow leaves were sampled as both attached to the tree (foliage) and as freshly fallen leaf litter on the ground. Red leaves that were still attached to the tree could not be sampled as they were out of reach of the pole pruner, and so were collected only on the ground. Three sugar maple seedlings from the understory, rooted in the forest floor (FH horizon), were also collected in September of 2010. Sugar maple xylem exudates (saps) were collected in April of 2011 during early, middle, and late harvest season from four individual adult sugar maple trees located within the study plot. All saps were collected with polyethylene trace metal clean spouts and pails (Dominion & Grimm Inc., Montréal, Québec). Saps were filtered and refrigerated for transport, and kept refrigerated during storage.

In addition to the field study samples, two sugar maple seedlings were cultivated *in vivo* at the Université du Québec à Montréal (UQAM) to compare findings for sugar maples growing naturally in the field to those growing in a laboratory-controlled setting. The seedlings were grown from non-germinated seeds in a finely crushed 3:1 mixture of acid washed quartz and basalt. A Mg-free standard Hoagland-type solution served as the nutrient supply to the seedlings, making the basalt and the original seed stores the only Mg source available to the seedlings during their growth. The seedlings were watered with 30 ml of the Mg-free nutrient solution every other day. The seedlings were harvested after five months of growth. The quartz/basalt growth mixture was sampled for bulk digestion and sequential leaching.

2.3. Tree biomass, Mg contents and uptake estimations

Allometric equations (reported in Lambert et al., 2005) for estimating the aboveground dry biomass compartments of sugar maple were applied using the DBH measurements recorded during sampling to calculate the total woody component biomass (stemwood and bark) as well as tree crown biomass (foliage and branches) of the SM3 tree in the study plot. The basal area of the study plot is 19.2 m^2 ha^{-1} and the DBH data for the remaining trees (both sugar maples and the other tree species) was also measured to determine the total inventory of Mg and Ca in the aboveground vegetation using average stemwood and foliage concentrations from Table 1 and estimates for Mg concentrations in bark and branches provided in the literature (Chatarpaul et al., 1985).

3. ANALYTICAL METHODS

3.1. Sample laboratory preparation

All samples were transported to a class 10,000 trace metal clean room at the Saskatchewan Isotope Laboratory

(SIL) for elemental and isotopic preparation. Solutions were filtered with a 0.45 μm polycarbonate membrane. Filters were pre-cleaned with 200 ml of ultrapure 0.3 N HNO_3, followed by a rinse with 200 ml of ultrapure water (18.2 MΩ cm). Filter blanks for Mg in the initial HNO_3 and subsequent ultrapure water rinses were 0.005 μg/ml and 0.0008 μg/ml, respectively.

Prior to acid digestion, all vegetation samples were oven dried at 50 °C for 48 h and dry masses were recorded. Vegetation samples were digested in ultrapure 15 N HNO_3 using polytetrafluoroethylene (PTFE) beakers covered with PTFE 'watch glasses', heated to 130 °C for 72 h. Following digestion, the sample solutions were dried at 80 °C and reconstituted in a final sample stock solution volume of 30 ml in 0.3 N HNO_3. Dried sap samples were treated with a mixture of high purity 30% hydrogen peroxide (H_2O_2) and 15 N HNO_3, and refluxed for an additional 24 h at 130 °C to assist in the degradation of complex organics. All sample solutions were then transferred to trace metal clean fluorinated ethylene propylene (FEP) bottles and exposed to simultaneous 185 nm and 254 nm ultraviolet (UV) radiation for a minimum of 72 h to assist in the degradation of residual organics in solution prior to elemental and Mg isotopic analysis. Clear solutions were obtained following UV exposure.

Whole leaf digestions of foliage and litter samples were carried out in duplicate. Stemwood whole-core samples were rinsed with ultrapure water to remove any surface particulates prior to being dried. Fine roots (< 2 mm) were rinsed and ultrasonicated in ultrapure water to remove any traces of soil from the root surface prior to being dried. Roots were visually inspected under a binocular microscope to check for attachment of surface particles (none were observed). Approximately 30 ml of each sap sample was used for elemental and isotopic analysis (0.4–1.5 g dried material). An additional aliquot of each sap was analyzed for sugar content (% Brix) using a Hanna HI96811 digital refractometer. The sampled seedlings from the study plot were rinsed with ultrapure water. The roots were cleaned following the previously described method. One seedling was acid digested whole, while the other two were sectioned by root (fine root and radicle), stem and leaves.

Soils were oven-dried in the laboratory at 50 °C for 48 h, and then gently disaggregated to break up coarse pieces to a ≤2 mm fraction that was assumed to be representative of the bulk soil. Solid pieces larger than 2 mm were removed prior to the sequential chemical leach. Approximately 3 g samples of the forest floor (FH horizon), and Bf-BC and C mineral soil horizons were subjected to a sequential chemical leach following protocols described in Bélanger and Holmden (2010) and Holmden and Bélanger (2010). The sequential extractions used in this study are as follows: (1) 30 ml 0.1 N $BaCl_2$ solution in a 50 ml acid cleaned centrifuge tube, (2) 30 ml 0.1 N HCl at room temperature (20–21 °C), (3) 30 ml 1 N HNO_3 at room temperature, and (4) 15 N HNO_3 at 80 °C for ~10 h. For each of the first three steps of the extraction procedure, solutions were gently shaken for two hours. The $BaCl_2$ extractions were subsequently treated with an ultrapure $NaSO_4$ solution to remove Ba as insoluble $BaSO_4$. Magnesium isotope fractionation is not expected during this step due to the very high solubility of $MgSO_4$. Finally, a 150 mg aliquot of each residue was acid digested in a 2.5:1 mixture of concentrated HF–HNO_3 at ~120 °C for 48 h, and then refluxed in 6 N HCl several times after dissolution to remove fluorides. In addition, untreated samples from each soil horizon were bulk digested using HF–HNO_3 acids and refluxed several times with 6 N HCl. A finely powdered sample of anorthosite bedrock was also subjected to the sequential extraction procedure, as was the quartz/basalt growth mixture used in the laboratory pot experiment.

All sequential extraction solutions were filtered with trace metal clean 0.2 μm Teflon membrane syringe filters. The solutions were then transferred into acid cleaned FEP bottles and treated extensively with UV radiation (until the solutions cleared), followed by dry-down and reconstitution in 0.3 N HNO_3 for elemental analysis, which also

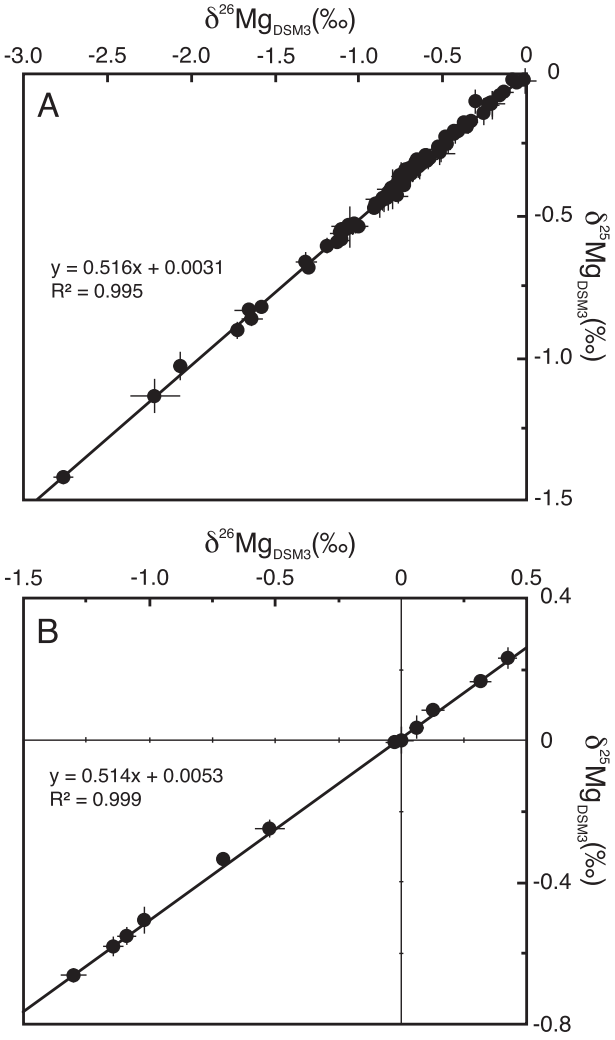

Fig. 3. Three-isotope plots for data on samples from the HEW field site in Table 1 (A), and data on samples from the laboratory pot experiments in Table 2 (B). Error bars shown are ±2 s.e. in the cases where the sample was analyzed during one mass spectrometry session and ±2σ in cases where the sample was analyzed in more than one mass spectrometry session.

served as a stock solution for further purification of Mg from matrix elements prior to mass spectrometry. The 0.1 N $BaCl_2$ extraction serves as a proxy for exchangeable cations, including Mg, Ca, and Sr. Drouet et al. (2005) proposed that the 0.1 N HCl leach dissolves calcite, although Miller et al. (1993) initially proposed this treatment as an effective simulation of the weathering signature of the anorthosite bedrock. The 1 N HNO_3 leach is believed to release some Mg from phyllosilicates (e.g., chlorite, biotite, vermiculite) and amphibole (Nezat et al., 2007, 2008; Bélanger and Holmden, 2010). The 15 N HNO_3 treatment leaches more resilient minerals, such as feldspars, but mostly causes a more complete degradation of phyllosilicates. The residues following the concentrated HNO_3 leach were completely digested with concentrated HF–HNO_3 acids and refluxed several times with 6 N HCl in order to release Mg in feldspars.

3.2. Elemental concentration, δ^{26}Mg and $^{87}Sr/^{86}Sr$ analyses

Vegetation digests were analyzed for trace and major elements by Perkin Elmer Inductively Coupled Plasma Optical Emissions Spectrometer (ICP-OES) using a 5–8 point calibration curve in the University of Michigan Biogeochemistry and Environmental Isotope Geochemistry Laboratory (BEIGL), with analytical uncertainties generally less than ±10% (2σ). All other sample solutions were analyzed by Thermo Scientific Element 2 HR-ICP-MS at the University of Michigan Keck Elemental Geochemistry Laboratory (KEGL), with analytical uncertainties generally less than ±5% (2σ).

Aliquots of each sample solution corresponding to 30 μg of Mg were purified using gravity-flow cation exchange columns packed with 2 ml of BioRad AG MP-50 resin. Some samples with lower concentrations of Mg (e.g., rainwater) were processed at the 10 μg level. Most Mg samples were eluted through two sets of cation exchange columns, as described in Kimmig and Holmden (2017), with the exception of those that were notably high in transition metals (soil and rock sequential extractions and digests). Due to the high Fe content of the soil digests and sequential leaches, these solutions were dissolved in 6 N HCl and eluted through an anion exchange column (0.5 ml BioRad AG 50X8) to remove both Fe and Mn from the sample solution prior to cation exchange chemistry for the separation of Mg, then passed through the standard two column separation procedure. The total procedural blank for the Mg purification procedure was < 16 ppb.

Samples of approximately 1 ppm Mg dissolved in 0.3 N HNO_3 were measured using a Thermo Scientific Neptune MC-ICP-MS instrument, housed in the Saskatchewan Isotope Laboratory (SIL), using specifications as described in Kimmig and Holmden (2017). Data are reported in the conventional delta notation as permil (‰) level differences in the $^{26}Mg/^{24}Mg$ ratio of the sample relative to the Dead Sea Mg metal standard (DSM3) (Galy et al., 2003). The $^{25}Mg/^{24}Mg$ ratios were also measured to show that the data are unaffected by isobaric interferences (Eq. (2), where x = 25 or 26; Fig. 3a, b). The long-term precision and accuracy of the measurements was monitored between differently

Table 2
Detailed Mg isotope data, Ca, Mg, and Sr concentrations as well as Ca/Mg, Mg/Sr, and Sr/Ca ratios for samples grown during the laboratory-controlled pot experiment using a Mg-free Hoagland solution and the quartz/basalt growth mixture digest/extracts. Prepared Mg solutions were analyzed within the same tuned sessions with errors denoted by 2 standard errors of the mean (2s.e.)

Sample ID	Sample type	Sample description	Dry mass (g)	N	δ^{26}Mg (‰DSM3)	2 s.e.	δ^{25}Mg (‰DSM3)	2 s.e.	$\Delta^{25}Mg$ [a]	Ca (ppm)	Mg (ppm)	Total Mg (μg)	Sr (ppm)	Fe (ppm)	Ca/Mg (mol/mol)	Mg/Ca (mol/mol)	Mg/Sr (mol/mol)	Sr/Ca (mmol/mol)	Fe/Mg (mol/mol)
Vegetation																			
V79	Sugar maple	Seed	0.044	3	−1.14	0.04	−0.59	0.03	0.00	44,419	1761	77.3	207		15.3	0.065	30.7	2.13	
V80	Sugar maple	Seed	0.064	4	−1.30	0.05	−0.67	0.02	0.01	19,969	2693	172	67.5		4.50	0.222	144	1.55	
		Average	*0.05*		*−1.22*		*−0.63*				*2227*	*125*							
		2σ	*0.03*		*0.23*		*0.11*				*1317*	*134*							
V81	Sugar maple	Roots	0.022	4	−0.02	0.04	−0.01	0.01	0.00	11,319	2240	49.9	16.4		3.06	0.326	493	0.662	
V82	Sugar maple	Leaves	0.073	4	0.01	0.05	0.00	0.04	−0.01	8191	238	17.3	9.28		20.9	0.048	92.4	0.518	
V83	Sugar maple	Stem	0.020	4	−0.52	0.06	−0.25	0.02	0.02	89,694	7100	141	93.7		7.66	0.131	273	0.478	
		Whole (calculated)	0.115		−0.35		−0.17			22,868	1812	208	25.2		7.66	0.131	259	0.505	
		Seed (estimated) [b]	*(0.05)*								*(1386)*	*(69.3)*							
V84	Sugar maple	Whole Seedling	0.071	4	−0.70	0.03	−0.34	0.02	0.03	30,962	2210	157	26.0		8.49	0.118	306	0.385	
		Seed (estimated) [b]	*(0.05)*								*(2300)*	*(115)*							
Growth mix extracts																			
S13	Quartz/Basalt	Bulk digest		4	0.13	0.05	0.08	0.02	0.01	2354	3535		12.8	8518	0.404	2.48	998	2.48	1.05
S13	Quartz/Basalt	0.1 N $BaCl_2$ Leach		4	−1.01	0.01	−0.51	0.04	0.02	206	5.51		9.28	1.69	22.6	0.044	2.14	20.7	0.134
S13	Quartz/Basalt	0.1 N HCl Leach		4	−1.08	0.04	−0.55	0.02	0.01	435	135		0.635	237	1.96	0.510	764	0.668	0.766
S13	Quartz/Basalt	1 N HNO_3 Leach		4	0.07	0.03	0.03	0.03	0.00	51.6	140		0.114	410	0.223	4.48	4433	1.01	1.27
S13	Quartz/Basalt	15 N HNO_3 Leach		4	0.32	0.04	0.16	0.02	0.00	116	1727		0.401	4354	0.041	24.5	15,540	1.58	1.10
S13	Quartz/Basalt	Residue digest		4	0.43	0.04	0.23	0.03	0.01	1799	860		11.6	2328	1.27	0.788	268	2.94	1.18

[a] Calculated using methods from Young and Galy (2004).
[b] Estimated dry masses (g), Mg concentrations (ppm), and total Mg content (μg) for the planted seed for each of the seedlings. See main text and Fig. S1 for more details.

tuned analytical sessions using interlaboratory standard Cambridge-1 (CAM1) with a δ^{26}Mg value of -2.62 ± 0.08‰ (2σ, n = 123). A similar estimate of external precision is found in repeated measurements of an internal standard (Alfa Aesar Specpure) yielding -3.80 ± 0.11‰ (2σ, n = 116). From these data, the overall external precision of the analyses is estimated to be approximately ±0.10‰ (2σ). In addition, four sample solutions were processed as duplicates through the entire Mg separation and isotope analysis procedure (indicated as 'Mg duplicate' in Table 1). In instances where sample material was digested, purified, and measured more than once, 'duplicate digest' is indicated in Table 1. Uncertainties associated with the measurements of samples within the same mass spectrometry session are reported as two standard errors of the mean (2s.e.), whereas errors from data collected over multiple mass spectrometry sessions are reported as two standard deviations (2σ) of the mean.

$$\delta^{x}Mg_{smp} = \left(\frac{(^{x}Mg/^{24}Mg)_{smp}}{(^{x}Mg/^{24}Mg)_{DSM3}} - 1 \right) \times 1000 \quad (2)$$

A single measurement of $^{87}Sr/^{86}Sr$ was performed on precipitation collected during Hurricane Irene using methods as described in Bélanger and Holmden (2010).

4. RESULTS

The total range in δ^{26}Mg values measured in the field study is 2.75‰ (Table 1; Fig. 3a). All samples are mass dependently fractionated, as indicated by the positive correlation between δ^{26}Mg and δ^{25}Mg values with a slope of 0.516 ± 0.006 (2σ) (Fig. 3a), which compares favorably with the theoretical slope of 0.521 for equilibrium isotope fractionation and 0.511 for kinetic isotope fractionation (Young and Galy, 2004). The total range in δ^{26}Mg values measured in the pot experiment is 1.72‰ (Table 2; Fig. 3b). The pot experiment samples also exhibit mass dependent behavior with a slope of 0.514 ± 0.010 (2σ) (Fig. 3b). Deviations from the terrestrial mass fractionation line are reported as Δ^{25}Mg' values in Tables 1 and 2.

4.1. Plant tissues and saps

Isotopic and elemental data for field collected vegetation are listed in Table 1. The average δ^{26}Mg value for fine roots is -0.60 ± 0.34‰ (2σ, n = 2), and the average Mg concentration is 1015 μg/g. Stemwood δ^{26}Mg values gave an average δ^{26}Mg value of -0.70 ± 0.19‰ (2σ, n = 2) and an average Mg concentration of 174 μg/g. Foliage exhibits the greatest variability in δ^{26}Mg values, ranging between −1.32‰ and −0.86‰. Categorized by leaf color, and whether the leaves were attached to the tree at the time of sampling or collected as fresh litterfall, the autumn 2010 sampling period gave the following average δ^{26}Mg values and Mg concentrations: (1) red leaf litterfall (-1.19 ± 0.36‰, 2σ, n = 2) and 1089 μg/g, (2) green (autumn) leaves (-1.12 ± 0.20‰, 2σ, n = 2) and 1613 μg/g, (3) yellow/green leaves (-0.98 ± 0.34‰, 2σ, n = 2) and 1124 μg/g, (4) yellow leaves (-0.96 ± 0.22‰, 2σ, n = 2) and 1578 μg/g, and (4) yellow leaf litterfall (−0.90‰) and 970 μg/g. Green leaves from the same tree (SM3) sampled the following spring yielded the highest δ^{26}Mg value of -0.27 ± 0.38‰ (2σ, n = 2) and an average Mg concentration of 1303 μg/g. The pattern that emerges from these data is that leaves are isotopically heavy in the spring, lighten during the summer, and become heavier again during autumnal senescence. The isotopic changes are accompanied by increasing Mg concentration in leaves leading up to senescence, with decreased concentrations following abscission.

The complete digest of a sugar maple seedling harvested from the study site yielded a δ^{26}Mg value of −0.60‰. Two other seedlings were sectioned before analysis, revealing decreasing δ^{26}Mg values in tissues that formed along the transpiration stream with $\delta^{26}Mg_{roots} > \delta^{26}Mg_{stems} > \delta^{26}Mg_{leaves}$ (Table 1). The weighted average δ^{26}Mg values for the reconstructed whole seedlings are −0.66‰ and −0.73‰, which is similar to the −0.60‰ value for the completely digested seedling.

The Mg allometry for the studied sugar maple tree (SM3) in the study plot is listed in Table 3. Stemwood and bark contain 57% of the Mg in sugar maple (33% and 24%, respectively), with foliage and branches containing the remainder (20% and 23%, respectively). The allometric equations used in these calculations (Lambert et al., 2005) do not take into account the belowground root biomass. Considering that roots may contain up to ~15% of the mass of woody tissue in sugar maple (Whittaker et al., 1974), we reapportioned this amount of Mg to the roots, which reduced the amount of Mg in stemwood and bark to ~50% (29% and 20%, respectively), and the Mg in foliage in branches to ~36% Mg (16% and 19%, respectively). The total aboveground mass of Mg and Ca in all of

Table 3
Magnesium concentrations in sugar maple tree 3 (SM3) components used to estimate aboveground Mg compartments in the HEW using equations in Lambert et al. (2005). Values shown in parentheses represent ±2σ errors.

Sugar maple – SM3 (*Acer saccharum* Marsh.)	Mg (g/kg)	Dry biomass (kg)	Mg per compartment (g)	Total Mg (%)
Stemwood	0.174[a] (0.17)	28.3	4.92	33%
Stembark	0.64[b] (0.12)	5.50	3.52	24%
Branches	0.42[b] (0.08)	8.19	3.44	23%
Foliage	1.4[a] (0.55)	2.00	2.81	20%
DBH (cm)	10.2[a]			

[a] Data collected during this study and provided in Table 1 and the main text.
[b] Data reported in Chatarpaul et al. (1985).

the trees in the study plot was also calculated, yielding 3068 g (126 mol) of Mg and 36,004 g (898 mol) of Ca, which gives a molar Mg/Ca ratio of 0.14.

Sugar maple saps collected at the beginning, middle, and end of the standard springtime harvesting season in 2011 yielded δ^{26}Mg values ranging between −1.10‰ and −0.79‰, with an average value of -0.95 ± 0.24‰ (2σ, n = 11) and average Mg concentration of 274 μg/g.

4.2. Water samples

Isotopic and elemental data for bulk precipitation, throughfall, stream water, and soil solutions are listed in Table 1, and illustrated in Fig. 2. Precipitation ranges between −1.73‰ and −1.58‰, with an average δ^{26}Mg value of -1.66 ± 0.20‰ (2σ, n = 2) and an average Mg concentration of 0.057 μg/ml. Hurricane Irene, which passed through the HEW in August of 2011, gave a δ^{26}Mg value of -2.22 ± 0.15‰ (2σ, n = 2) and an average Mg concentration of 0.041 μg/ml. Two throughfall samples yielded quite different δ^{26}Mg values of −2.76‰ and −1.30‰, but similar Mg concentrations, averaging 0.066 ± 0.02 μg/ml. Stream water gave an average δ^{26}Mg value of -0.59 ± 0.22‰ (2σ, n = 8) with an average Mg concentration of 0.36 ± 0.10 μg/ml, which falls within the uncertainty of all three lysimeter depth soil solutions which gave an average δ^{26}Mg value of -0.65 ± 0.15‰ (2σ, n = 14), and an average Mg concentration of 0.39 ± 0.27 μg/ml. There was no discernable difference in δ^{26}Mg values for stream waters sampled at high and low flows. By contrast, the δ^{26}Mg value of Lac Triton was lower when measured at low water level (−1.64‰) and higher when measured at a high water level (−1.13‰). Both measurements are conspicuously lower than the stream waters and soil solutions, but are similar to precipitation values (−1.73 to −1.57‰).

4.3. Soils and bedrock

Isotopic and elemental data for soil and bedrock digestions and sequential leach extractions are listed in Table 1. Effective cation exchange capacities (CEC_e) for different soil horizons are listed in Table 4. Duplicate digestions of the anorthosite bedrock gave an average δ^{26}Mg value of -0.21‰ ± 0.00‰ (2σ, n = 2). The soils, however, are much lower in δ^{26}Mg value yielding −0.64‰ for the FH horizon, −0.75‰ for the Bf-BC horizon, and −0.71‰ for the C horizon.

The equivalent CEC_e of the FH horizon is 16.5 cmol kg^{-1}. The CEC_e of the underlying mineral soils is much smaller, yielding 0.415 cmol kg^{-1} for the Bf-BC horizon, and 0.353 cmol kg^{-1} for the C horizon. The largest cache of plant-available Mg is therefore hosted at the surface (Thiffault et al., 2006). The δ^{26}Mg values for the CEC_e in each soil horizon (equivalent to the 0.1 N $BaCl_2$ extracts) are from top to bottom, −0.59‰ for the FH, −1.65‰ for the Bf-BC, and −2.07‰ for the C. The δ^{26}Mg values of the 0.1 N HCl extracts are −0.74‰ for the FH, and −0.80‰ for the C. The low Mg concentration of the 0.1 N HCl extract of the Bf-BC horizon did not permit its iso-

Table 4
Dry sample mass (g), total solution volume (ml), effective cation exchange capacity (CEC_e), δ^{26}Mg values (‰DSM3), and elemental concentrations cmol kg^{-1} for soil horizons and bedrock 0.1 N $BaCl_2$ leach solutions in the HEW study plot.

Sample ID	Horizon	Sample Mass (g)	Total Sol'n (ml)	CEC_e [a] (cmol kg^{-1})	δ^{26}Mg (‰DSM3)	Na (cmol kg^{-1})	Mg (cmol kg^{-1})	Al (cmol kg^{-1})	K (cmol kg^{-1})	Ca (cmol kg^{-1})	Mn (cmol kg^{-1})	Fe (cmol kg^{-1})
S06	Forest floor (FH)	3.06	24.8	16.5	−0.59	0.036	0.852	1.01	0.318	14.2	0.028	0.017
S10	Bf-BC	3.02	29.0	0.415	−1.65	0.016	0.006	0.282	0.007	0.101	0.002	0.001
S11	C	2.88	29.6	0.353	−2.07	0.022	0.008	0.177	0.009	0.129	0.006	0.001
R01	Anorthosite	2.84	32.2	1.51	−1.10	0.161	0.102	0.014	0.066	1.16	0.002	0.000

[a] Calculated using equations and conversion factors provided in Hendershot et al. (2007) and defined as Σ of Ca^{2+}, Mg^{2+}, K^+, Na^+, Fe^{2+}, Al^{3+}, and Mn^{3+}; H^+ was not included in the calculation.

topic measurement. The δ^{26}Mg values of the 1 N HNO_3 extracts are −0.30‰ for the FH, −0.66‰ for the Bf-BC, and −0.66‰ for the C. The δ^{26}Mg values of the 15 N HNO_3 extracts are −0.43‰ for the FH, −0.08‰ for the Bf-BC, and −0.03‰ for the C. The δ^{26}Mg values for the HF–HNO_3 digestion of the residues are −0.37‰ for the FH, −0.69‰ for the Bf-BC, and −0.65‰ for the C. The fraction of Mg liberated by each of the sequential leaches is listed in Table 5.

4.4. Pot experiments

Isotopic and elemental data for the pot experiments are listed in Table 2 and illustrated in Fig. 4. Two sugar maple seeds were measured, yielding an average δ^{26}Mg value of -1.22 ± 0.22‰ (2σ, n = 2). Seedling roots (fine roots and radicle combined) yielded a δ^{26}Mg value of −0.02‰, while the stem and leaves yielded −0.52‰ and +0.01‰, respectively. The complete digestion of a whole seedling yielded a δ^{26}Mg value of −0.70‰. The δ^{26}Mg values for the sequential extraction of the quartz/basalt soil mixture yielded −1.01‰ for 0.1 N $BaCl_2$ extract, −1.08‰ for the 0.1 N HCl extract, +0.07‰ for the 1 N HNO_3 extract, +0.32‰ for the 15 N HNO_3 extract, and +0.43‰ for the HF–HNO_3 digestion of the residue. The δ^{26}Mg value of a bulk HF–HNO_3 digest of the quartz/basalt soil yielded +0.13‰. The mass fractions of Mg liberated by the applied sequential leaches of the quartz/basalt mixture are listed in Table 5.

Table 5
Summary of the Mg mass fractions for each sequential leach of the mineral soil horizons in the HEW study plot and the quartz/basalt growth mixture in the laboratory pot experiment.

HEW soils						
Bf-BC Horizon	0.1 N $BaCl_2$	0.1 N HCl	1 N HNO_3	15 N HNO_3	Residue digest	Weighted bulk
δ^{26}Mg (‰DSM3)	−1.65	–	−0.66	−0.08	−0.69	−0.59
Mg (ppm)	0.77	1.14	24.7	1270	6341	
Mass fraction (Mg)	0.001	0.001	0.019	0.979		
C Horizon						
δ^{26}Mg (‰DSM3)	−2.07	−0.80	−0.66	−0.03	−0.65	−0.54
Mg (ppm)	1.03	1.84	31.9	1533	7163	
Mass fraction (Mg)	0.001	0.001	0.020	0.978		
Pot experiment						
Quartz/Basalt	0.1 N $BaCl_2$	0.1 N HCl	1 N HNO_3	15 N HNO_3	Residue digest	Weighted bulk
δ^{26}Mg (‰DSM3)	−1.01	−1.08	0.07	0.32	0.43	0.00
Mg (ppm)	5.51	135	140	1727	860	
Mass fraction (Mg)	0.003	0.067	0.070	0.860		

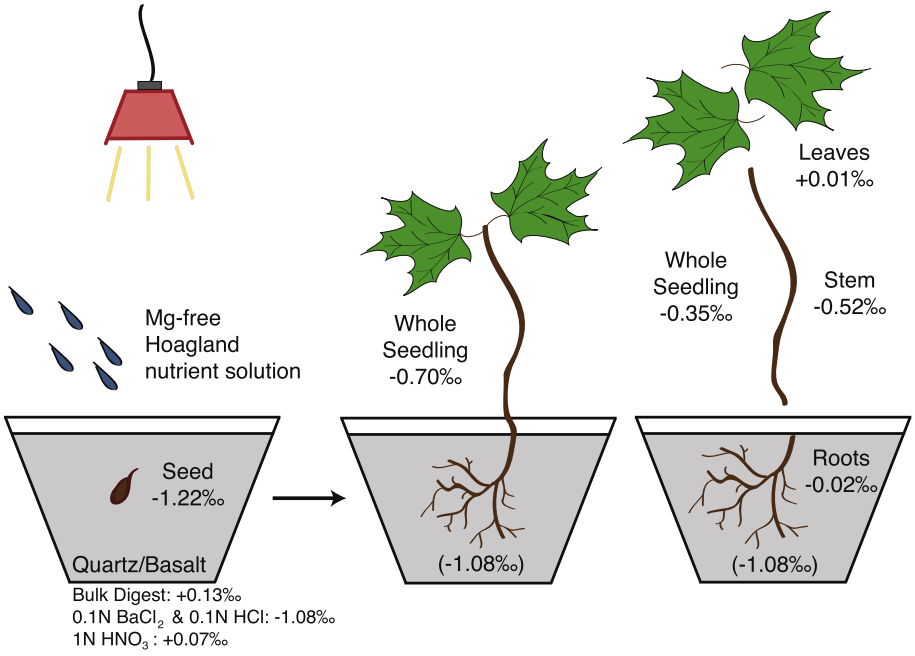

Fig. 4. δ^{26}Mg values for the seedlings grown in the laboratory in a quartz/basalt soil. One of the seedlings was harvested and digested whole. The other seedling was sectioned into roots, stem, and leaves, and the whole plant δ^{26}Mg is the reconstructed weighted average value based on the measurements of the three tissues. The plant-available pool of Mg for the seedlings is denoted as (−1.08‰) in each pot.

5. DISCUSSION

5.1. Precipitation

The HEW records the lowest δ^{26}Mg value for precipitation to date, yielding -2.22 ± 0.15‰ (2σ, n = 2), collected during hurricane Irene in August of 2011 (Table 1; Fig. 2). This compares to an average background value for rainfall at the study site of -1.66 ± 0.21‰ (2σ, n = 2) (Table 1; Figs. 2 and 5). Hurricane Irene was named as the first hurricane of the Atlantic Ocean 2011 season, which made landfall in North Carolina. From there, the storm moved north-northwest along the east coast of the United States, eventually crossing the international boundary with Canada where it delivered large amounts of precipitation to southern Québec (Fig. 6). Surprisingly, there appears to be little seawater-derived Mg in Irene at the study site. A case in point, coastal precipitation near Santa Cruz, California has a δ^{26}Mg value of -0.79 ± 0.05‰ (2σ, n = 5) (Tipper et al., 2010), which is consistent with a Mg source from sea spray. The conspicuous absence of sea salt aerosols in Irene is confirmed with a $^{87}Sr/^{86}Sr$ measurement of 0.7089, which is significantly lower than the seawater ratio of 0.7092, but falls within the range of $^{87}Sr/^{86}Sr$ ratios in background precipitation previously reported for the study site, averaging 0.7104 ± 0.0030 (2σ, n = 14) (Bélanger et al., 2012).

The low δ^{26}Mg signature of Irene precipitation (−2.22‰) is reminiscent of the low δ^{26}Mg values that characterize marine carbonate minerals such as aragonite (~−1.8‰), calcite (~−2.0 to −4.0‰) (Saenger and Wang, 2014), and dolomite (-1.8 ± 1.1‰) (Geske et al., 2015), thus prompting consideration of whether carbonate dust may be the source of dissolved Mg in precipitation delivered by Irene. Another possibility is Mg extracted from leaves at the top of the canopy by wind and rain. Bulk leaves, however, are not as low in δ^{26}Mg value as Irene precipitation, and so there would have to be a mechanism favoring the preferential leaching of Mg in chlorophyll (~−3.7‰) (Section 5.3) from the leaves. Both hypotheses

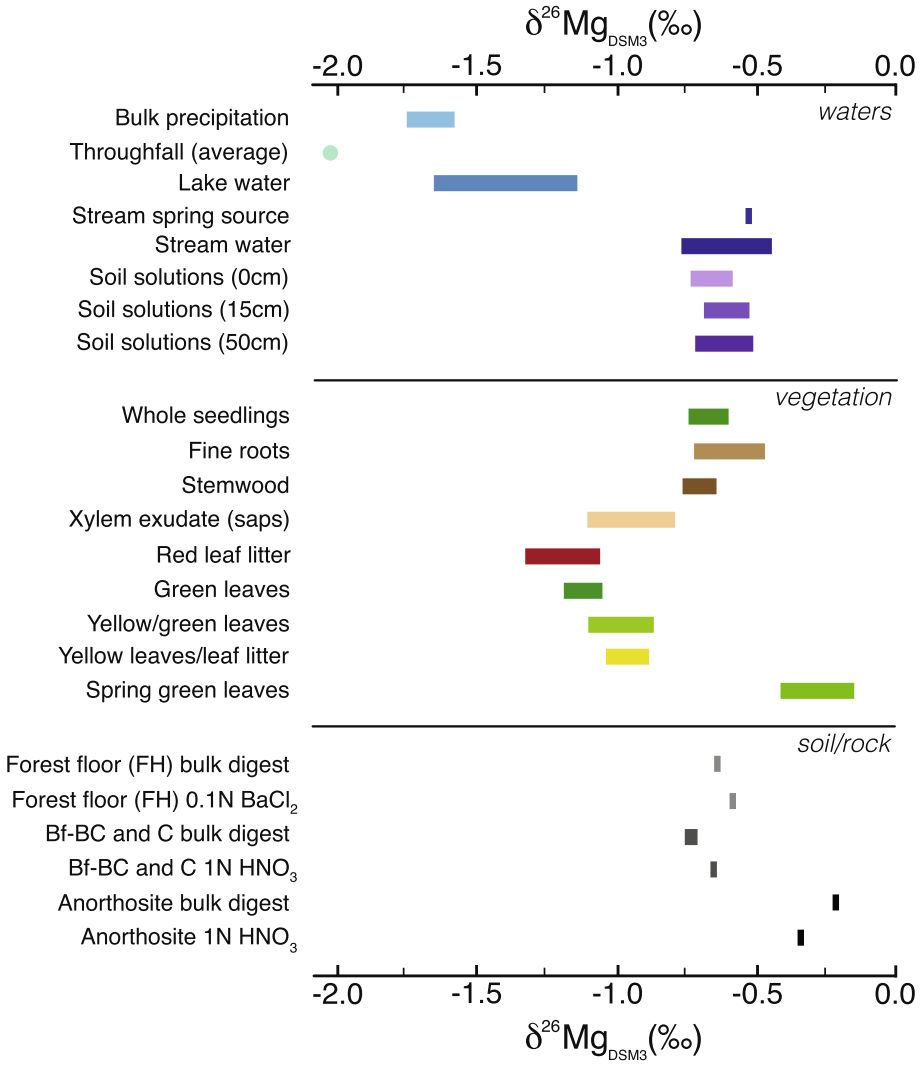

Fig. 5. Ranges of variation in δ^{26}Mg values for components of the forest Mg cycle in the HEW field site. Throughfall is shown as an average δ^{26}Mg value.

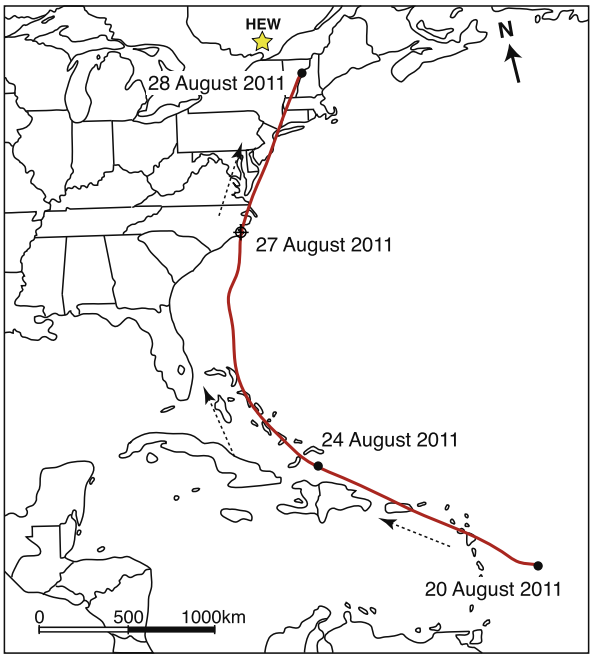

Fig. 6. Hurricane Irene storm track from August of 2011, based on data provided in Avila and Cangialosi (2011). The target symbol denotes landfall on August 27th, 2011 near Cape Lookout, North Carolina. The HEW is shown as a yellow star. (For interpretation of the references to colour in this figure legend, the reader is referred to the web version of this article.)

are consistent with the low δ^{26}Mg value measured in throughfall at the study site (*avg.* −2.03‰) (Fig. 5). Despite the low values measured in this study, a survey of the literature shows that the median value for δ^{26}Mg in precipitation is −0.80‰ (n = 23) (Table S3), which is nearly identical to the seawater δ^{26}Mg value of −0.83 ± 0.09‰ (2σ, n = 90) (Ling et al., 2011).

5.2. Source of Mg in Lac Triton

Despite the low average δ^{26}Mg value (−1.66 ± 0.21‰, 2σ, n = 2) for precipitation at the study site, there is little evidence for an atmospheric fingerprint of Mg in soil, stream, and spring waters, averaging −0.63 ± 0.18‰ (2σ, n = 21). The exception is Lac Triton with an average δ^{26}Mg value of −1.38 ± 0.73‰ (2σ, n = 2) (Table 1; Figs. 1 and 2). Normally, soil solutions (−0.65 ± 0.15‰) would be expected to drain into the lake, as they appear to do for the stream (−0.60 ± 0.23‰). However, the sampling of Lac Triton was performed in the epilimnion (uppermost layer) of the lake, and there is the possibility that we sampled a stratified layer of lake water that is predominantly sourced from precipitation falling directly over the lake. If this is correct, a simple mass balance calculation reveals that ~72% of the Mg in this layer is from rainfall.

5.3. Mg isotope fractionation during leaf senescence

Studies have demonstrated that 6–25% of total Mg in plants is associated with chlorophyll (Marschner, 1995). Another 5–10% of Mg in leaves is immobilized in the pectate of cell walls or precipitated as soluble salts (phosphates). The remaining 60–90% is extractable with water (Marschner, 1995). From these numbers, it can be seen that plants require Mg for purposes other than the synthesis of chlorophyll (Wilkinson et al., 1990; Marschner, 1995; Epstein and Bloom, 2005; Barker and Pilbeam, 2007). Low δ^{26}Mg values have been reported in the majority of Mg isotope studies that have measured chlorophyll from various sources (Galy et al., 2001; Young and Galy, 2004; Black et al., 2006, 2008; Ra and Kitagawa, 2007; Ra et al., 2010). Although chlorophyll was not isolated and measured in this study, sugar maple leaves are lower in δ^{26}Mg than other tree tissues, and they reach their lowest values in the autumn when chlorophyll concentration is highest. This points to chlorophyll having a low δ^{26}Mg value in sugar maple, in agreement with findings from other plants. However, there are exceptions, as English Ivy and marine phytoplankton appear to sequester heavy Mg isotopes during chlorophyll synthesis (Black et al., 2007; Ra and Kitagawa, 2007). It was suggested by Black et al. (2006) that the low δ^{26}Mg value for chlorophyll-a might be due to the preferential binding of light Mg isotopes to the protein backbone of Mg-chelatase. A similar preference is seen for light isotope partitioning onto AG 50W-X12 cation exchange resin used to purify Mg isotopes prior to mass spectrometry (Chang et al., 2003). We can estimate the δ^{26}Mg value of chlorophyll in sugar maple from material balance considerations. Assuming that the difference in δ^{26}Mg values between spring (−0.27‰) and autumn (green) foliage (−1.12‰) is due to the accumulation of chlorophyll in leaves over the growing season (Lewandowska and Jarvis, 1977), and that the fraction of Mg in chlorophyll in leaves approaches the 25% maximum near the end of the growing season (Marschner, 1995), material balance considerations put the δ^{26}Mg value of chlorophyll at ~−3.7‰ in sugar maple. This is in line with δ^{26}Mg values for chlorophyll-a in spinach (−3.01‰) and for *Anacystis nidulans* algae (−3.55‰) (Ra and Kitagawa, 2007).

The finding that spring leaves have higher δ^{26}Mg values than fine roots casts doubt on the xylem behaving as a chromatographic column for the fractionation of Mg isotopes in tissues formed along the transpiration stream. To investigate this further, we looked for evidence that Mg isotopes were fractionated in xylem sap flowing during the spring of 2011. The low average δ^{26}Mg value of sap (−0.95 ± 0.24‰) is inconsistent with fractionation at the root tips favoring uptake of heavy Mg isotopes from soils, nor can it be explained by the absence of fractionation at the root tips because the solutions have higher δ^{26}Mg values of ~−0.65‰.

Senescence is the final stage of leaf development, signaling the onset of winter. It is marked by changes in leaf color and the breakdown of chloroplasts and chlorophyll (Langmeier et al., 1993; Noodén et al., 1997; Decoteau, 2005; Pessarakli, 2016). One of the processes occurring during leaf senescence is the translocation of base cations into perennial tissues of the stemwood, providing over-wintering species with a cache of nutrients that can be utilized the following spring when the canopy is reconstructed (Collier and

Thibodeau, 1995). If chlorophyll is isotopically light, then senescence should drive leaves toward higher δ^{26}Mg values, which is what we generally observe with changes from green to yellow leaves. However, red leaves have unexpectedly low δ^{26}Mg values, lower even than green leaves. The red pigment, anthocyanin, belongs to a class of flavonoids which are water soluble vascular pigments responsible for red/violet colors in many flowers, fruits, and leaves of higher plants (Davies, 2004). Anthocyanin production starts shortly after chlorophyll degradation begins, often triggered by environmental stresses and high irradiance (Hoch et al., 2001, 2003). Exposure to strong sunlight can causes photoinhibition, which impairs the capacity of leaves to photosynthesize. The production of anthocyanin serves as a photoprotective 'sunscreen' that shields the photosynthetic apparatus from damage, thus enabling photosynthetic activity to continue late into the senescence period (Hoch et al., 2001, 2003). This photoprotective mechanism in the red leaves suggests that they are actively photosynthesizing in the autumn, and this may explain their low δ^{26}Mg values compared to green leaves sampled at the same time. In addition, the green leaves may have already experienced partial chlorophyll breakdown and translocation of light Mg isotopes into stemwood, when the leaves were sampled in the early fall. This raises the question, if the main cache of re-translocated Mg in the spring is from chlorophyll breakdown in the fall, then why do spring leaves start out with such a high δ^{26}Mg value? Is there a large fractionation factor upon forming leaves in the spring? Or, does the Mg used to grow the leaves in spring come from another source? We cannot answer this question at the present time, but the large Mg isotope fractionations will be useful for addressing these questions in future detailed studies that are process oriented.

5.4. Uptake fractionation of Mg isotopes by sugar maple

Holmden and Bélanger (2010) showed that tree fine roots preferentially take up light Ca isotopes, thus driving plant-available Ca in soils to higher δ^{44}Ca values. This finding has been replicated in a number of studies (Farkaš et al., 2011, Cobert et al., 2011; Hindshaw et al., 2011, 2013; Schmitt et al., 2012, 2013; Bagard et al., 2013; Bullen and Chadwick, 2016). Magnesium isotopes appear to be more complicated. Generally, authors have presented evidence that fractionation during uptake of Mg into plants is opposite to that of Ca (Black et al., 2008; Tipper et al., 2010, 2012b; Bolou-Bi et al., 2010, 2012; Opfergelt et al., 2014; Uhlig et al., 2017). A notable exception is the Dahurian larch tree (*Larix gmelinii*), which appears to take up Mg from soil solutions without fractionation (Mavromatis et al., 2014) (Table S1). While there is plenty of evidence for within-tree fractionation in the sugar maples from the HEW field site, we find no evidence for uptake-related fractionation of Mg isotopes between the sugar maple trees and the plant-available Mg in the soils. For example, the average δ^{26}Mg value of fine roots collected from the FH horizon is -0.60 ± 0.34‰ (2σ, n = 2), which is nearly identical to the 0.1 N $BaCl_2$ leach of the same horizon soil, yielding -0.59 ± 0.02‰ (2s.e.). A number of more aggressive extractions yielded similar δ^{26}Mg values (Tables 1 and 5), as does the average δ^{26}Mg value for all soil solutions measured over the course of this study, yielding -0.65 ± 0.15‰ (2σ, n = 14).

As an additional and more definitive test of the absence of uptake-related fractionation in sugar maple in the HEW field site, three seedlings rooted in the litter of the forest floor (the FH horizon) were analyzed. One completely digested seedling growing in this layer yielded -0.60 ± 0.02‰ (2s.e) (Table 1; Fig. 2), which is nearly identical to the 0.1 N $BaCl_2$ leach of the FH horizon, yielding -0.59 ± 0.02‰ (2s.e.). Two other seedlings were dissected into roots, stems, and leaves. The roots and stems were similar, yielding -0.41 ± 0.17‰ (2σ, n = 2), and the leaves were lower, yielding -0.78 ± 0.11‰ (2σ, n = 2), which is consistent with the magnitude and direction of within-tree Mg isotope fractionation observed in mature sugar maple trees. However, the reconstructed weighted average δ^{26}Mg values of the two seedlings yields -0.66‰ and -0.73‰, similar to the δ^{26}Mg value of the whole-digested seedling (-0.60‰). Combining the data from all three seedlings yields an average whole seedling δ^{26}Mg value of -0.66 ± 0.13‰ (2σ), which is again very close to the -0.59 ± 0.02‰ (2s.e.) value of the $BaCl_2$ extract of the FH horizon, and indistinguishable from the average δ^{26}Mg value for the soil solutions collected from directly below the FH horizon in the 0 cm lysimeter, which is also -0.66 ± 0.13‰ (2σ, n = 6). In fact, the average δ^{26}Mg value for all of the soil solutions is similar, yielding -0.65 ± 0.15‰ (2σ, n = 14) (Table 1; Figs. 2 and 5). Regardless of how the calculation is performed, the conclusion remains the same, there is no observable evidence for uptake-related fractionation of Mg isotopes in sugar maple in the HEW field site.

Stemwood, bark, and branches account for ~80% of the Mg in mature sugar maple (Table 3). The immobilization of Mg in stemwood, branches, and to a lesser extent, bark, constitutes a net sink of Mg over the time scale of forest growth because it is not returned annually to the forest floor as litterfall. Although bark and branches were not measured in this study, the average δ^{26}Mg value for stemwood (-0.70 ± 0.19‰) is unfractionated relative to the plant-available Mg in the soils. This finding suggests that in the absence of data on whole plants, the δ^{26}Mg value of stemwood may be used to estimate the whole-plant δ^{26}Mg value. Literature data on δ^{26}Mg values in whole plants and stemwood are compiled in Table S1, along with best estimates of δ^{26}Mg values for plant-available Mg in the soils in which the plants grew. These data are used to calculate the average uptake-related fractionation factor ($\Delta^{26}Mg = \delta^{26}Mg_{plant} - \delta^{26}Mg_{source}$) for a variety of plants and locations, yielding $+0.14 \pm 0.51$‰ (2σ, n = 10). For comparison, the $\Delta^{26}Mg_{plant\text{-}source}$ value for field stands of sugar maple measured in this study is -0.01 ± 0.08‰ (2σ). Considering the practical difficulties of instrumenting and sampling field sites to collect representative data for the estimation of the uptake-related Mg isotope fractionation factor in plants, and the small average size of the fractionations reported in the literature, it seems that Mg cycling in forests might contribute very little to lower-than-bedrock δ^{26}Mg values in rivers draining silicate watersheds.

If there is no uptake-related fractionation of Mg isotopes in sugar maple in the HEW field site, then the annual return flux of Mg to the forest floor should be unfractionated as well, considering that the Mg reservoir in stemwood is unfractionated. Indeed, the δ^{26}Mg value of a complete digest of the FH horizon (the litter layer comprising the forest floor) yields -0.64 ± 0.07‰ (2s.e.), thus validating the mass balance constraint. However, green, yellow, and red leaves measured during autumnal senescence yielded much lower δ^{26}Mg values averaging -1.04 ± 0.30‰ (2σ, n = 9) (Table 1). The highest δ^{26}Mg values were measured in yellow-green and yellow leaves, yielding δ^{26}Mg values of -0.86‰ and -0.87‰, respectively (Table 1), but these are still too low to correct the imbalance in δ^{26}Mg values between the forest floor and the canopy. Fractionation during litter degradation can be ruled out as a potential explanation because the soil water filtering through the FH horizon is unfractionated compared to the litter, yielding -0.66 ± 0.13‰ (2σ, n = 6). Instead, we can think of two sources of sampling bias that might explain the discrepancy. First, we may have undersampled the range of Mg isotope fractionation that occurs during leaf senescence, with the implication being that the autumn leaves were collected before the peak in chlorophyll breakdown and the preferential transfer of light Mg isotopes into the overwintering stemwood. Second, there is a component of the litter and the canopy that we did not measure, the most likely one being seeds. If seeds are isotopically heavier than foliage, this could account for the imbalance between autumnal leaves and the litter of the forest floor. Indeed, in their study of hydroponically grown wheat, Black et al. (2008) showed that seeds have higher δ^{26}Mg values than foliar tissue. Seeds are also high in Mg concentration. The seeds measured for the pot experiments (Section 5.7) were purchased from a seed company, and as such their δ^{26}Mg values are not relevant to the Mg cycle in the HEW, but their concentrations may serve as reference values, yielding 1761 and 2693 μg/g (Table 2), which is consistent with literature values of ~3000 μg/g (Cleavitt et al., 2011).

5.5. Atmospheric dust and mineral weathering contributions of Mg to the forest Mg cycle

Using $^{87}Sr/^{86}Sr$ as a tracer, Bélanger et al. (2012) argued that only ~15% of the plant-available Ca in the HEW is from atmospheric sources. The remaining 85% is released during weathering of soil minerals, mostly calcite and apatite, as determined from sequential leaches of the mineral soil in the C horizon. Calcite and apatite contain plenty of Ca, but very little Mg. Dolomite has equal abundances of Ca and Mg but there is no evidence that dolomite is present in the mineral soil. The molar Mg/Ca ratio of the 0.1 N HCl leach of the C horizon is ~0.004, which fingerprints calcite rather than dolomite. On the other hand, it might be difficult to detect dolomitic dust from atmospheric sources due to its high solubility in the soils (see Section 5.1). Chlorite, biotite, and vermiculite are more reliable sources of weathered Mg, which XRD reveals are present in the mineral soil. Indeed, a positive covariance between $^{87}Sr/^{86}Sr$ and Mg/Sr ratios in the 1 N and 15 N HNO_3 leaches of the C horizon (Bélanger et al., 2012) appears to target these minerals, with the Mg primarily sourced from chlorite and the radiogenic ^{87}Sr from biotite, and possibly vermiculite, which can be a weathering product of biotite.

In this study, we can distinguish chlorite from biotite/vermiculite on the basis of its potentially low δ^{26}Mg value, as shown in a granodiorite weathering experiment by Ryu et al. (2011) who studied time-dependent changes in δ^{26}Mg, $\delta^{44/40}$Ca, and $\delta^{44/42}$Ca values in the output of a column reactor subjected to weak acid attack (0.1 N HCl). The granodiorite employed for the experiment was composed of plagioclase (29.8 wt.%), quartz (29.0 wt.%), K-feldspar (10.4 wt.%), biotite (8.4 wt.%), chlorite (1.5 wt.%), hornblende (1.0 wt.%), titanite (0.9 wt.%), epidote (0.7 wt.%), apatite (0.3 wt.%), and calcite (0.2 wt.%). What is relevant to this study is the fact that ~96% of the Mg in the granodiorite is distributed between just three minerals, biotite (−0.29‰), hornblende (−0.32‰) and chlorite (−1.82‰), with their respective δ^{26}Mg values listed in parentheses. The whole-rock value of the granodiorite is −0.77‰, which is low on account of the large fraction of Mg contributed by chlorite. The bulk digest of the C mineral soil in this study yields a similarly low δ^{26}Mg value of −0.71‰, which we also attribute to chlorite based on XRD analysis of the B horizon soil yielding 19% chlorite, 5.5% biotite/vermiculite, and 4% hornblende (Bélanger et al., 2012). Using the stoichiometry of chlorite, biotite, and hornblende in Ryu et al. (2011), 79% of the Mg in the in the HEW soil would be in chlorite, ~ 14% would be in biotite/vermiculite, and ~8% would be in hornblende. Assuming that biotite, vermiculite, and hornblende have mantle like δ^{26}Mg values ~−0.25‰, a simple material balance calculation predicts a value of −0.78‰ for chlorite in the study setting.

One additional finding that merits discussion is the low δ^{26}Mg values for the 0.1 N $BaCl_2$ extracts performed on the Bf-BC and C horizons (−2.07 to −1.65‰, respectively) (Tables 4 and 5; Fig. 7). These low values are not observed in the 1 N HNO_3 treatments of the same soils, which yielded -0.66 ± 0.0‰ (2σ, n = 2), nearly identical to the bulk digest of the forest floor (−0.64‰), the 0.1 N $BaCl_2$ extract of the forest floor (−0.59‰), all soil solutions

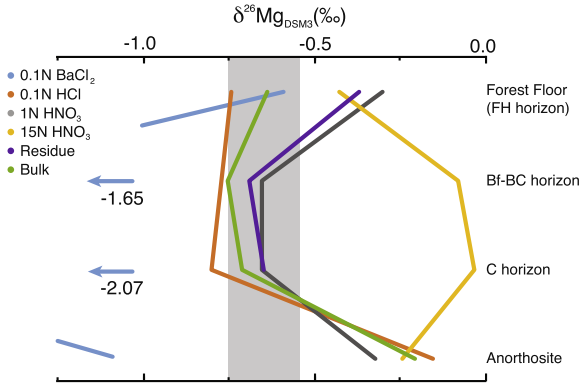

Fig. 7. δ^{26}Mg profiles for sequential leaches and digests of the soil at three depths corresponding to the FH, Bf-BC, and C horizons. The gray bar corresponds to the range of δ^{26}Mg values in soil solutions collected by the lysimeters.

(-0.65 ± 0.15‰, 2σ), and the HF-HNO_3 digest of the mineral soil in the C horizon (−0.71‰) (Table 1; Figs. 5, 7 and 8), which we have hypothesized reflects the large fraction of chlorite (−0.78‰) in the soils. We do not have a good explanation for the low δ^{26}Mg values for the two $BaCl_2$ extracts of the mineral soils but note that Wimpenny et al. (2014) reported low δ^{26}Mg values for Mg that is weakly adsorbed to surface and interlayer sites of illite, montmorillonite, and kaolinite (<−1.5‰). Only in the structural sites of clay minerals did the authors find evidence for the often-cited heavy isotope enrichment of Mg isotopes in clays. Ryu et al. (2016) reported similar findings.

In addition to the intrinsic value of Mg isotopes as a tracer, it is also worth considering the molar Mg/Ca ratios between the vegetation and soil. The Mg/Ca ratio of the 1 N HNO_3 leach of the Bf-BC and C horizons (0.17 ± 0.01, 2σ) is similar to the Mg/Ca ratio in leaves (0.15 ± 0.05, 2σ), the bulk digest of the forest floor (0.18), soil solutions (0.18 ± 0.11, 2σ), and the entire aboveground biomass of the study plot (0.14) (Fig. 8), as determined from the Mg and Ca allometry (see Section 4.1). These data indicate that seven times more Ca than Mg is required to support forest growth. It raises the question, why would the 1 N HNO_3 attack of the C horizon mineral soil, which is often used to estimate mineral weathering contributions to plant-available soil pools, release Mg and Ca in the exact proportions needed by the plants? In the discussion above, the 1 N HNO_3 leach was used to identify chlorite as the main source of weathered Mg to plant-available soil pools, with subsidiary biotite and vermiculite, but this does not explain the source of Ca. Typically, soil minerals are: (1) high in Ca and low in Mg (calcite, apatite), (2) high in both Ca and Mg (dolomite), or (3) high in Mg and low in Ca (chlorite, biotite). Recognizing that it is unlikely that the weathering of Ca and Mg bearing minerals will synchronize with the nutritional needs of the forest, it is suggested that the 1 N HNO_3 leach is not signaling the dissolution of primary igneous minerals, but rather secondary minerals in the soils that formed during weathering. Courchesne et al. (2005) report that the HEW soils contain up to 20% clays in the B and C horizons, and it is well known that chlorite and biotite can transform into smectites (beidellite or montmorillonite) or vermiculite as a result of acid leaching (Churchman and Lowe, 2012) in acidic podzols. Furthermore, the Mg released by an acid attack of these secondary minerals could not have been inherited from biotite (which typically yields a high mantle-like δ^{26}Mg value). It therefore seems likely that these secondary minerals have captured Mg and Ca filtering down through the soil profile from the degradation of the litterfall layer of the forest floor.

This finding warrants caution in the application of the 1 N HNO_3 leach as a treatment for probing the elemental and isotopic compositions of the mineral soil (Blum et al., 2002; Nezat et al., 2007, 2008; Bélanger and Holmden, 2010; Holmden and Bélanger, 2010; Bélanger et al., 2012). Van der Heijden et al. (2017) reached a similar conclusion in their soil column study of Mg and Ca cycling using ^{26}Mg and ^{44}Ca enriched isotopic tracers, showing that Ca and Mg in soil solutions can diffuse into non-crystalline soil phases that are not easily released by conventional weak

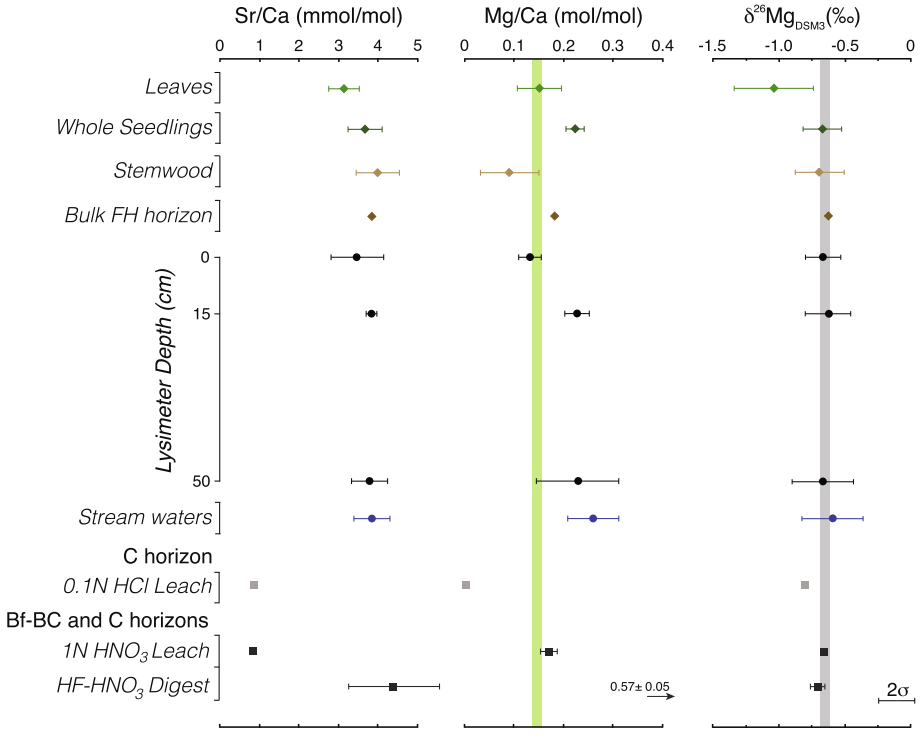

Fig. 8. Soil depth water profiles of average Sr/Ca (mmol/mol), Mg/Ca (mol/mol), and δ^{26}Mg (‰DSM3) and selected sequential extractions of the C mineral soil, compared to vegetation Error bars are ±2σ for each sample grouping. The vertical green bar denotes the Mg/Ca molar ratio of the aboveground biomass compartment (0.14), as calculated in the main text. The vertical gray bar indicates the δ^{26}Mg value of the cache of recycled Mg (−0.65‰) in the study site.

extraction techniques, such as NH_4-acetate and $BaCl_2$. A more aggressive attack, such as 1 N HNO_3, is required to release these cations. The results of their study and the present one supports the idea that through multiple successive generations of forests, a cache of nutrient Mg and Ca is created in the soils that is close to the ideal ratio of the two ions needed to support optimal forest growth (Fig. 8). The nutrient cache is maintained by tight recycling of these elements over timescales of thousands of years.

5.6. Mg isotope signature of environmental waters exported from the watershed

Stream water exhibits fairly uniform δ^{26}Mg values (-0.60 ± 0.23‰, 2σ) at all times of the year, as well as at high and low flows. The dissolved Mg in the stream water is isotopically heavier than bulk precipitation and throughfall (Table 1; Fig. 2), but similar to δ^{26}Mg values in soil solutions collected at all depths in the soil profile, yielding -0.65 ± 0.15‰ (2σ) (Fig. 5). Bélanger et al. (2012) measured stream water $^{87}Sr/^{86}Sr$ ratios from samples collected at three times of the year yielding 0.70764, 0.70761, and 0.70791 for low, medium, and high stream flows, respectively. They attributed the shift to lower $^{87}Sr/^{86}Sr$ ratios at low stream flows to anorthosite weathering, and high $^{87}Sr/^{86}Sr$ ratios at high stream flows to larger Sr inputs from soil solutions. Bolou-Bi et al. (2012) reported a similar effect for δ^{26}Mg values in a stream from a forested catchment in the Vosges Mountains in northeast France.

Ultimately, the stream waters in the HEW reflect Mg returned to the soil pool by litterfall and recycled by vegetation, with minimal contributions from anorthosite bedrock weathering and bulk precipitation. Silicate weathering in the mineral soil also contributes Mg to the stream. However, Bélanger et al. (2012) estimated with the SAFE model that (at most) the flux of Mg liberated from silicate weathering is 10% of the total concentration of base cations in the exchangeable pool (~100 mol ha^{-1} yr^{-1}). Atmospheric Mg deposition contributes ~25 mol of ha^{-1} yr^{-1}, and it was estimated for other HEW study plots that 400 mol ha^{-1} yr^{-1} of Mg returns annually to the forest floor as litterfall (Bélanger et al., 2002). The average uptake rate of Mg for the HEW plot in this study is $\sim 296 \pm 184$ mol ha^{-1} yr^{-1}, based on the calculated inventory of Mg stored in the mature tree foliage at the time of sampling (and using different allometric equations than Bélanger et al., 2002). This demonstrates that the litterfall return flux of Mg is nearly four times larger than the soil mineral weathering Mg-flux to the vegetation. This is a substantial amount of Mg returned to the soil pool in the HEW each year, which is consistent with the finding that soil pools at each lysimeter depth record identical δ^{26}Mg values.

5.7. Sugar maple seedlings and Mg uptake, insights from a laboratory pot experiment

The field-based finding, that there is no apparent isotopic fractionation of Mg during uptake into sugar maple trees, is not validated by the laboratory pot experiment. The sugar maple seedlings grown in the laboratory are enriched in heavy Mg isotopes compared to the plant-available Mg in the mixture of crushed basalt and quartz that was prepared as an artificial growth substrate. The complete digestion of one of the seedlings gave a δ^{26}Mg value of −0.70‰ while the plant-available Mg released by the 0.1 N $BaCl_2$ and 0.1 N HCl extractions of the artificial soil gave similar δ^{26}Mg values of −1.01‰ and −1.08‰, respectively (Table 2). These are somewhat surprising results given that basalt typically has a δ^{26}Mg value of −0.2 to −0.4‰ (Teng, 2017). It indicates that the basalt contains secondary clay minerals, and possibly chlorite that formed through water-rock interaction and/or metamorphism. The amount of Ca released in the 0.1 N HCl leach also suggests that there is calcite in the sample. The stronger 1 N HNO_3 leach yielded a δ^{26}Mg value of +0.07‰, which is closer to basalt, confirming that the inferred calcite and chlorite are trace constituents of the basalt. Despite their low abundance, these trace minerals appear to control the δ^{26}Mg value of the plant-available Mg in the growth medium. The 'apparent' fractionation factor is ~+0.4‰, calculated from the difference in δ^{26}Mg values between the whole seedling (−0.70‰) and the weighted average δ^{26}Mg value of plant-available Mg in the artificial soil (−1.08‰) (Table S1). This value, however, assumes that all of the Mg in the seedling is derived from the artificial soil, but there is also the original inventory of Mg in the seed from which the plant grew that must be taken into account.

Two sugar maple seeds analyzed in this study gave an average Mg concentration of 2227 ± 1317 μg/g (2σ) and an average δ^{26}Mg value of -1.22 ± 0.23‰ (2σ) (Table 2). Two others were planted and grown into seedlings. A bulk digest of the smaller seedling yielded a δ^{26}Mg value of −0.70‰. The larger seedling was sectioned into roots (fine root and radicle), stem, and leaves, yielding a reconstructed weighted average δ^{26}Mg value of −0.35‰ (Fig. 4). Comparing the Mg concentrations of the seeds and seedlings (Table 2), it is clear that each seedling contains a large fraction of Mg from their respective seeds. Accordingly, each seedling is a mixture of Mg from the seeds and soil. We can calculate the fraction of soil-derived Mg in each seedling using mass balance, and the following assumptions: (1) both seeds from which the seedling grew had the same δ^{26}Mg values of -1.22 ± 0.23‰, (2) both seedlings grew from the same pool of plant-available Mg in the artificial soil, and (3) have the same uptake-related Mg isotope fractionation factor. We then choose an initial Mg concentration for the planted seeds (2300 μg/g) that satisfies the condition that both seedlings have δ^{26}Mg values of −1.22‰ when the uptake fraction of soil-derived Mg is zero (Fig. S1). Assuming that no Mg was lost from the seedlings during their growth, the fraction of soil-derived Mg is 0.27 in the whole seedling and 0.45 in the reconstructed seedling. The calculations make it clear that most of the Mg in the seedlings is from the original seeds at the time of harvesting (Table 2; Fig. S1). Plotting the mass fractions of soil derived Mg against the δ^{26}Mg values of the whole-seedlings (Fig. S1), it can be seen that when the soil Mg fraction is 1.0, the soil-derived δ^{26}Mg value is +0.72‰. This is considerably higher than the −1.08‰ value of the plant-available Mg in the soils, thus indicating a large uptake-related Mg

isotope effect of +1.80‰. This is the largest uptake-related fractionation factor reported in the literature. Even if the isotopically heavier Mg released by the 1 N HNO_3 leach is combined with the Mg released by the less aggressive treatments, the plant-available Mg yields a δ^{26}Mg value of −0.51‰, and the uptake-related Mg isotope fractionation factor is still quite large at ~+1.2‰.

The contrasting findings between field and laboratory studies regarding uptake-related Mg isotope fractionation in sugar maple is surprising, but it is not unprecedented. There have been reported $\Delta^{26}Mg_{plant\text{-}source}$ values ranging between +0.2‰ and +1.21‰, calculated from hydroponic experiments growing wheat, rye, and clover (Black et al., 2008; Bolou-Bi et al., 2010). A survey of the literature shows that the average uptake-related fractionation factor in laboratory studies is larger than the field-based average, +0.59 ± 0.39‰ (2s.e.) and +0.16 ± 0.14‰ (2s.e.), respectively (Table S1). This discrepancy requires an explanation. The most obvious one relates to the sterile growth media used in laboratory experiments, which do not contain mycorrhizal fungi. These fungi have been shown to facilitate uptake of nutrients into the fine roots of plants while the fine roots, in turn, exude carbohydrates to help support the growth of the fungi in what is widely considered to be a mutualistic symbiotic relationship (Smith and Read, 2008). For example, it has been reported that arbuscular mycorrhizae in the roots of sugar maple help the trees survive in acidic podzol environments where they would not normally thrive (Klironomos, 1995). Furthermore, Jones (1998) cautions that laboratory-grown vegetation, especially vegetation grown hydroponically, can exert stresses not usually seen with vegetation grown on natural soils due to morphological and physiological changes to the roots that negatively affect nutrient uptake. Plants grown on sterile soil often fail to thrive. Only two of the six sugar maples seeded at the beginning of this study survived, and surviving plants exhibited signs of stress under the applied growth conditions and were quickly harvested before they also perished.

Although we tentatively identify the activities of the mycorrhizal fungi as being responsible for the lack of Mg isotope fractionation in the field stands of sugar maple in the HEW, studies have shown that ectomycorrhizal fungi can fractionate Mg isotopes. Fahad et al. (2016) cultured ectomycorrhizal fungi and non-mycorrhizal fungi in the laboratory on growth substrates including granite, the forest floor of a boreal podzol, and a Modified Melin-Norkrans (MMN) fungal culture medium, in order to measure the Mg isotopic fractionation effects associated with fungal uptake of Mg. They found that the magnitude and sign of the Mg isotope fractionation depended on the species of fungi cultured and the culture medium. For example, fungi colonizing granite largely sequestered light isotopes, while fungi colonizing a forest floor substrate showed smaller fractionations, with some species even switching to the uptake of heavy Mg isotopes. Non-mycorrhizal fungi predominantly sequestered heavy Mg isotopes with the exception of *Heterobasidion parviporum*, which exhibited a light Mg isotope preference, or no fractionation at all (Fahad et al., 2016).

As previously mentioned, sugar maples form symbiotic relationships with arbuscular mycorrhizae; these fungi penetrate the fine roots (Klironomos, 1995). Ectomycorrhizal fungi, on the other hand, cover the surfaces of roots (Smith and Read, 2008; Landeweert et al., 2001). It is therefore tempting to conclude that the lack of uptake-related Mg isotope fractionation in field stands of sugar maple might be due to the colonization by arbuscular mycorrhizae, which presumably pass unfractionated Mg isotopes from soil solutions to the fine roots of the maple trees. Pokharel et al. (2017) recently concluded that uptake-related fractionation of Mg isotopes by fine roots could, in some cases, reflect processes driven by the mycorrhizal fungi. Wheat grass is also known to form symbiotic relationships with arbuscular mycorrhizae, and the common practice of inoculating wheat fields with these fungi helps to reduce drought stress and increase overall productivity of the crop (Al-Karaki et al., 2004). Black et al. (2008) found that wheat grass grown in a hydroponic nutrient solution favored the uptake of heavy Mg isotopes, but this finding may not describe the behavior of field grown wheat, by analogy with laboratory and field grown sugar maple trees in this study.

6. IMPLICATIONS AND CONCLUSIONS

Dissolved Mg in rainfall collected at a sugar maple dominated field site in southern Québec, Canada, gave a low δ^{26}Mg value, lower than trees and soils, but higher than leaf chlorophyll. The low value may be attributed to the dissolution of carbonate dust in the atmosphere, as carbonate minerals are known to have low δ^{26}Mg values. However, interactions between the forest canopy and the atmosphere also warrants consideration, as throughfall can be lower in δ^{26}Mg value than rainfall, possibly indicative of a preferential leaching of chlorophyll-derived Mg from leaves during precipitation.

Translocation of Mg in sugar maple causes significant within tree isotopic fractionation, as evidenced by differences in δ^{26}Mg values between roots, stemwood, and foliage in juvenile (seedlings) and mature trees. Green leaves are lower in δ^{26}Mg value than stemwood and fine roots, and chlorophyll is inferred to be isotopically light compared to the whole leaves on the basis that newly erupted leaves in the spring are isotopically heavier than mature leaves, and that chlorophyll concentration increases with leaf maturation. Leaves become isotopically heavy again during autumnal senescence, consistent with chlorophyll breakdown and translocation of the released Mg into the overwintering stemwood. Although this cache of Mg is assumed to be available for reuse the following spring, there is no isotopic evidence that it is used in the growth of spring leaves, which have high δ^{26}Mg values ranging between −0.4‰ and −0.13‰, whereas the value for chlorophyll is estimated to be −3.7‰. Senescent leaves collected and measured in the early autumn are lighter than the litterfall layer of the forest floor horizon, indicating that: (1) senescent leaves were collected before most of the chlorophyll-bound Mg was recovered into the stemwood, and/or (2)

there is an isotopically heavy component of Mg in the litter (and in the trees) that wasn't sampled, such as seeds.

Despite the wide range of Mg isotope fractionation between different tree tissues in both field and laboratory grown sugar maple trees, only the laboratory grown specimens fractionated Mg isotopes during uptake of Mg from plant-available pools in the soils. This finding agrees with literature studies of other laboratory grown plants (Black et al., 2008; Bolou-Bi et al., 2010), but this is the first study to show that the same plants growing on natural soils in the field do not fractionate Mg isotopes. The difference is tentatively attributed to the arbuscular mycorrhizal fungi that naturally colonize the fine roots of field stands of sugar maple but were absent from the fine roots of sugar maple grown in the sterile soils of the pot experiments. Mycorrhizal fungi form symbiotic relationships with sugar maple, passing water and nutrients to the fine roots in exchange for carbohydrates formed by leaf photosynthesis. Fungal symbiosis enhances the fitness of sugar maple populations in nature, prompting the suggestion that a large uptake-related Mg isotope fractionation may be used as an isotopic fingerprint for stress in these trees. The absence of uptake-related Mg isotope fractionation in field grown sugar maple warrants caution when using laboratory grown plants as proxies for their field-grown counterparts. If it can be demonstrated that many other tree species from heavily populated forest biomes also do not fractionate Mg isotopes during uptake from soil solutions, then the forests growing in continental weathering environments, whose activities are known to accelerate mineral weathering, will have little or no impact on the δ^{26}Mg value of the weathering flux of Mg to the oceans. This, however, may not be true for Ca isotopes (e.g., Holmden and Bélanger, 2010; Farkaš et al., 2011, Cobert et al., 2011; Hindshaw et al., 2011, 2013; Schmitt et al., 2012, 2013; Bagard et al., 2013; Fantle and Tipper, 2014; Bullen and Chadwick, 2016), or the Mg/Ca molar ratio.

The Mg/Ca molar ratios of soil solutions and the first-order stream are nearly identical to the Mg/Ca ratio of the trees at the study site, indicating that plant-recycled fluxes of Mg and Ca completely mask the much smaller annualized input fluxes of Mg from atmospheric deposition and soil mineral weathering. This observation is further supported by the 1 N HNO_3 leach of the mineral soil in the C horizon, which yields the ~7:1 ratio of Ca to Mg observed in the trees at the study site. The similarity is attributed to the degradation of litter on the forest floor, which releases Mg and Ca that filters down through the soil profile to become trapped in secondary minerals. These findings warrant caution when using 1 N HNO_3 acid for simulating soil mineral weathering of parent material. The cache of recycled Mg has a δ^{26}Mg value (−0.65‰), which is too heavy to fingerprint atmospheric deposition (−1.6‰) and too light to fingerprint the commonly found ferromagnesian minerals in the studied soils, such as biotite and hornblende (~−0.25‰). We instead attribute this signature to the weathering of chlorite, which has been shown to have a low δ^{26}Mg value in a granodiorite studied by Ryu et al. (2011) and is also the most abundant Mg-bearing mineral in the HEW soils.

Lastly, there is no evidence that clays in this setting, which are known to take up heavy Mg isotopes, actually influence the δ^{26}Mg values of the soil solutions or first-order stream, despite their documented presence in the soils. Clay mineral fractionation is the most widely cited mechanism that has been offered to explain the lower-than-bedrock δ^{26}Mg values in streams and rivers draining silicate watersheds in regions with little or no vegetation. However, on the basis of the results presented in this study, more attention should be paid to the possibility that the lowering of riverine δ^{26}Mg values may also be due to preferential weathering of finely disseminated calcite in silicate rocks. This is particularly necessary in cool climates and regions with high physical erosion rates, such as rapidly uplifting mountain belts and glaciated catchments.

ACKNOWLEDGEMENTS

Thank you to the director and staff of the Station de biologie des Laurentides de l'Université de Montréal for allowing the use of their facilities as well as additional assistance in the field. Field work assistance was greatly appreciated from B. Brenna, K. Scheiderich, F. Bélanger, A. Collin, D. Caron, and E. Valiquette. Laboratory assistance from M. Nasreen, J. Rosen, B. Lafleur, T. Huston, J. Gleason, and M. Johnson was much appreciated. J. Kimmig is also thanked for editorial assistance. Lastly, we thank the associate editor A. Jacobson for his excellent handling of this manuscript, as well as three anonymous reviewers whose comments and criticisms helped to significantly improve the final draft. This work was supported by funds to C. Holmden and N. Bélanger from the Natural Sciences and Engineering Research Council of Canada (NSERC) Discovery grant program.

APPENDIX A. SUPPLEMENTARY MATERIAL

Supplementary data associated with this article can be found, in the online version, at https://doi.org/10.1016/j.gca.2018.03.020.

REFERENCES

Al-Karaki G., McMichael B. and Zak J. (2004) Field response of wheat to arbuscular mycorrhizal fungi and drought stress. *Mycorrhiza* **14**, 263–269.

Avila L. A. and Cangialosi J. (2011) Tropical cyclone report hurricane Irene (AL092011) 21–28 August 2011. National Hurricane Center. 45p.

Bagard M. L., Schmitt A. D., Chabaux F., Pokrovsky O. S., Viers J., Stille P., Labolle F. and Prokushkin A. S. (2013) Biogeochemistry of stable Ca and radiogenic Sr isotopes in a larch covered permafrost-dominated watershed of Central Siberia. *Geochim. Cosmochim. Acta* **114**, 169–187.

Barker A. V. and Pilbeam D. J. (2007) *Handbook of Plant Nutrition*. CRC Press, Taylor and Francis Group, p. 662p.

Bélanger N. and Holmden C. (2010) Influence of landscape on the apportionment of Ca nutrition in a Boreal Shield forest of Saskatchewan (Canada) using $^{87}Sr/^{86}Sr$ as a tracer. *Can. J. Soil Sci.* **90**, 267–288.

Bélanger N., Côté B., Courchesne F., Fyles J. W., Warfvinge P. and Hendershot W. H. (2002) Simulation of soil chemistry and nutrient availability in a forested ecosystem of southern Quebec – I. Reconstruction of the time-series files of nutrient cycling using the MAKEDEP model. *Environ. Model. Software* **17**, 427–445.

Bélanger N., Côté B., Fyles J. W., Courchesne F. and Hendershot W. H. (2004) Forest regrowth as the controlling factor of soil nutrient availability 75 years after fire in a deciduous forest of Southern Quebec. *Plant Soil* **262**, 363–372.

Bélanger N., Holmden C., Courchesne F., Côté B. and Hendershot W. H. (2012) Constraining soil mineral weathering $^{87}Sr/^{86}Sr$ for calcium apportionment studies of a deciduous forest growing on soils developed from granitoid igneous rocks. *Geoderma* **185–186**, 84–96.

Berner R. A. (1997) The rise of plants and their effects on weathering and atmospheric CO_2. *Science* **276**, 544–546.

Berner R. A., Lasaga A. C. and Garrels R. M. (1983) The carbonate-silicate geochemical cycle and its effect on atmospheric carbon dioxide over the past 100 million years. *Am. J. Sci.* **283**, 641–683.

Black J. R., Yin Q. Z. and Casey W. H. (2006) An experimental study of magnesium-isotope fractionation in chlorophyll-a photosynthesis. *Geochim. Cosmochim. Acta* **70**, 4072–4079.

Black J. R., Yin Q. Z., Rustad J. R. and Casey W. H. (2007) Magnesium isotopic equilibrium in chlorophylls. *J. Am. Chem. Soc.* **129**, 8690–8691.

Black J. R., Epstein E., Rains W. D., Yin Q. Z. and Casey W. H. (2008) Magnesium isotope fractionation during plant growth. *Environ. Sci. Technol.* **42**, 7831–7836.

Blum J. D., Gazis C. A., Jacobson A. D. and Chamberlain C. P. (1998) Carbonate versus silicate weathering in the Raikhot watershed within the High Himalayan Crystalline Series. *Geology* **26**, 411–414.

Blum J. D., Klaue A., Nezat C., Driscoll C. T., Johnson C. E., Siccama T. G., Eagar C., Fahey T. J. and Likens G. E. (2002) Mycorrhizal weathering of apatite as an important calcium source in base-poor forest ecosystems. *Nature* **417**, 729–731.

Bolou-Bi E. B., Poszwa A., Leyval C. and Vigiet N. (2010) Experimental determination of magnesium isotope fractionation during higher plant growth. *Geochim. Cosmochim. Acta* **74**, 2523–2537.

Bolou-Bi E. B., Vigier N., Poszwa A., Boudot J.-P. and Dambrine E. (2012) Effects of biogeochemical processes on magnesium isotope variations in a forested catchment in the Vosges Mountains (France). *Geochim. Cosmochim. Acta* **87**, 341–355.

Bolou-Bi E. B., Dambrine E., Angeli N., Pollier B., Nys C., Guerold F. and Legout A. (2016) Magnesium isotope variations to trace liming input to terrestrial ecosystems: a case study in the Vosges Mountains. *J. Environ. Qual.* **45**, 276–284.

Brenot A., Cloquet C., Vigier N., Carignan J. and France-Lanord C. (2008) Magnesium isotope systematics of the lithologically varied Moselle river basin, France. *Geochim. Cosmochim. Acta* **72**, 5070–5089.

Bullen T. and Chadwick O. (2016) Ca, Sr and Ba stable isotopes reveal the fate of soil nutrients along a tropical climosequence in Hawaii. *Chem. Geol.* **422**, 25–45.

Chang V. T.-C., Makishima A., Belshaw N. S. and O'Nions R. K. (2003) Purification of Mg from low Mg biogenic carbonates for isotope ratio determination using multiple-collector ICP-MS. *J. Anal. At. Spectrom.* **18**, 296–301.

Chapela Lara M., Buss H. L., Pogge von Strandmann P. A. E., Schuessler J. A. and Moore O. W. (2017) The influence of critical zone processes on the Mg isotope budget in a tropical, highly weathered andesitic catchment. *Geochim. Cosmochim. Acta* **202**, 77–100.

Chatarpaul L., Burgess D. M. and Methven I. R. (1985) Equations for estimating above-ground nutrient content of six eastern Canadian hardwoods. Inf. Rep. PI-X-55, Petawawa National Forestry Institute, Canadian Forestry Service, Chalk River, Ontario.

Churchman G. J. and Lowe D. J. (2012) Alteration, formation, and occurrence of minerals in soils. In Handbook of Soil Sciences 2nd Edition, Vol. 1: Properties and Processes (Eds. P. M. Huang, Y. Li, and M. E. Sumner) CRC Press, Taylor and Francis, Boca Raton, FL, USA pp. 20.1–20.72.

Cleavitt N. L., Fahey T. J. and Battles J. J. (2011) Regeneration ecology of sugar maple (*Acer saccharum*): seedling survival in relation to nutrition, site factors, and damage by insects and pathogens. *Can. J. For. Res.* **41**, 235–244.

Cobert F., Schmitt A.-D., Bourgeade P., Labolle F., Badot P.-M., Chabaux F. and Stille P. (2011) Experimental identification of Ca isotopic fractionations in higher plants. *Geochim. Cosmochim. Acta* **75**, 5467–5482.

Collier D. E. and Thibodeau B. A. (1995) Changes in respiration and chemical content during autumnal senescence of *Populus tremuloides* and *Quercus rubra* leaves. *Tree Physiol.* **15**, 759–764.

Courchesne F., Côté B., Fyles J. W., Hendershot W. H., Biron P. M., Roy A. G. and Turmel M.-C. (2005) Recent changes in soil chemistry in a forested ecosystem of southern Québec Canada. *Soil Sci. Soc. Am. J.* **69**, 1298–1313.

Davies K. M. (2004) *Plant Pigments and Their Manipulation. Annual Plant Reviews*. Blackwell, p. 368p.

Decoteau D. R. (2005) Principles of plant science: Environmental factors and technology in growing plants. Pearson Prentice Hall. 432 pp.

Derry L. A., Kurtz A. C., Ziegler K. and Chadwick O. A. (2005) Biological control of terrestrial silica cycling and export fluxes to watersheds. *Nature* **433**, 728–730.

Dessert C., Lajeunesse E., Lloret E., Clergue C., Crispi O., Gorge C. and Quidelleur X. (2015) Controls on chemical weathering on a mountainous volcanic tropical island: Guadeloupe (French West Indies). *Geochim. Cosmochim. Acta* **171**, 216–237.

Doig R. (1991) U-Pb Zircon dates of Morin anorthosite suite rocks, Grenville Province, Quebec. *J. Geol.* **99**, 729–738.

Drever J. I. (1994) The effect of land plants on weathering rates of silicate minerals. *Geochim. Cosmochim. Acta* **58**, 2325–2332.

Drouet Th., Herbauts J., Gruber W. and Demaiffe D. (2005) Strontium isotope composition as a tracer of calcium sources in two forest ecosystems in Belgium. *Geoderma* **126**, 203–223.

Emslie R. F. (1975) Major rock units of the Morin Complex, southwestern Quebec. Geol. Survey Canada Paper 74–48, 45 pp.

Epstein E. and Bloom A. J. (2005) *Mineral Nutrition of Plants: Principles and Perspectives*, 2nd ed. Sinauer Associates Inc., USA, p. 380p.

Fahad Z. A., Bolou-Bi E. B., Köhler S. J., Finlay R. D. and Mahmood S. (2016) Fractionation and assimilation of Mg isotopes by fungi is species dependent. *Environ. Microbiol. Rep.* **8**, 956–965.

Fantle M. S. and Tipper E. T. (2014) Calcium isotopes in the global biogeochemical Ca cycle: implications for development of a Ca isotope proxy. *Earth Sci. Rev.* **129**, 148–177.

Farkaš J., Déjeant A., Novák M. and Jacobsen S. B. (2011) Calcium isotope constraints on the uptake and sources of Ca2+ in a base-poor forest: a new concept of combining stable (δ44/42Ca) and radiogenic (εCa) signals.

Friedman R. M. and Martignole J. (1995) Mesoproterozoic sedimentation, magmatism, and metamorphism in the southern part of the Grenville Province (western Quebec): U-Pb geochronological constraints. *Can. J. Earth Sci.* **32**, 2103–2114.

Galy A., Belshaw N., Halicz L. and O'Nions R. (2001) High precision measurement of magnesium-isotopes by multiple-collector inductively coupled plasma mass spectrometry. *Int. J. Mass Spectrom.* **208**, 89–98.

Galy A., Yoffe O., Janney P., Williams R., Cloquet C., Alard O., Halicz L., Wadhwa M., Hutcheon I., Ramon E. and Carignan J. (2003) Magnesium-isotope heterogeneity of the isotopic standard SRM980 and new reference materials for magnesium isotope-ratio measurements. *J. Anal. At. Spectrom.* **18**, 1352–1356.

Geske A., Goldstein R. H., Mavromatis V., Richter D. K., Buhl D., Kluge T., John C. M. and Immenhauser A. (2015) The magnesium isotope (δ^{26}Mg) signature of dolomites. *Geochim. Cosmochim. Acta* **149**, 131–151.

Hendershot W. H., Lalande H. and Duquette M. (2007) Ion exchange and exchangeable cations. In Soil sampling and methods of analysis (Eds. M. R. Carter and E. G. Gregorich). CRC Press, Boca Raton, FL, USA, 10 pp.

Hindshaw R. S., Reynolds B. C., Wiederhold J. G., Kretzschmar R. and Bourdon B. (2011) Calcium isotopes in a proglacial weathering environment: Damma glacier, Switzerland. *Geochim. Cosmochim. Acta* **75**, 106–118.

Hindshaw R. S., Reynolds B. C., Wiederhold J. G., Kiczka M., Kretzschmar R. and Bourdon B. (2013) Calcium isotope fractionation in alpine plants. *Biogeochemistry* **112**, 373–388.

Hoch W. A., Zeldin E. L. and McCown B. H. (2001) Physiological significance of anthocyanins during autumnal leaf senescence. *Tree Physiol.* **21**, 1–8.

Hoch W. A., Singsaas E. L. and McCown B. H. (2003) Resorption protection. Anthocyanins facilitate nutrient recovery in autumn by shielding leaves from potentially damaging light levels. *Plant Physiol.* **133**, 1296–1305.

Holmden C. and Bélanger N. (2010) Ca isotope cycling in a forested ecosystem. *Geochim. Cosmochim. Acta* **74**, 995–1015.

Huang K.-J., Teng F.-Z., Wei G.-J., Ma J.-L. and Bao Z.-Y. (2012) Adsorption- and desorption controlled magnesium isotope fractionation during extreme weathering of basalt in Hainan Island, China. *Earth Planet. Sci. Lett.* **359–360**, 73–83.

Jacobson A. D. and Blum J. D. (2000) Ca/Sr and $^{87}Sr/^{86}Sr$ geochemistry of disseminated calcite in Himalayan silicate rocks from Nanga Parbat: Influence on river water chemistry. *Geology* **28**, 463–466.

Jacobson A. D., Blum J. D. and Walter L. M. (2002) Reconciling the elemental and Sr isotope composition of Himalayan weathering fluxes: Insights from the carbonate geochemistry of stream waters. *Geochim. Cosmochim. Acta* **66**, 3417–3429.

Jacobson A. D., Andrews M. G., Lehn G. O. and Holmden C. (2015) Silicate versus carbonate weathering in Iceland: new insights from Ca isotopes. *Earth Planet. Sci. Lett.* **416**, 132–142.

Jones D. L. (1998) Organic acids in the rhizosphere – a critical review. *Plant Soil* **205**, 25–44.

Kimmig S. R. and Holmden C. (2017) Multi-proxy geochemical evidence for primary aragonite precipitation in a tropical-shelf 'calcite sea' during the Hirnantian glaciation. *Geochim. Cosmochim. Acta* **206**, 254–272.

Klironomos J. N. (1995) Arbuscular mycorrhizae of *Acer saccharum* in different soil types. *Can. J. Bot.* **73**, 1824–1830.

Lambert M.-C., Ung C.-H. and Raulier F. (2005) Canadian national tree aboveground biomass equations. *Can. J. For. Res.* **35**, 1996–2018.

Landeweert R., Hoffland E., Finlay R. D., Kuyper T. W. and van Breemen N. (2001) Linking plants to rocks: ectomycorrhizal fungi mobilize nutrients from minerals. *Trends Ecol. Evol.* **16**, 248–254.

Langmeier M., Ginsburg S. and Matile Ph. (1993) Chlorophyll breakdown in senescent leaves: demonstration of Mg-dechelatase activity. *Physiol. Plant.* **89**, 347–353.

Lewandowska M. and Jarvis P. G. (1977) Changes in chlorophyll and carotenoid content, specific leaf area and dry weight fraction in Sitka spruce, in response to shading and season. *New Phytol.* **79**, 247–256.

Li W., Chakraborty S., Beard B. L., Romanek C. S. and Johnson C. M. (2012) Magnesium isotope fractionation during precipitation of inorganic calcite under laboratory conditions. *Earth Planet. Sci. Lett.* **333–334**, 304–316.

Li W., Beard B., Li C. and Johnson C. M. (2014) Magnesium isotope fractionation between brucite [$Mg(OH)_2$] and Mg aqueous species: Implications for silicate weathering and biogeochemical processes. *Earth Planet. Sci. Lett.* **394**, 82–93.

Ling M. X., Sedaghatpour F., Teng F. Z., Hays P. D., Strauss J. and Sun W. D. (2011) Homogenous magnesium isotopic composition of seawater: an excellent geostandard for Mg isotope analysis. *Rapid Commun. Mass Spectrom.* **25**, 2828–2836.

Liu G. E. and Côté B. (1993) Neutralization and buffering capacity of leaves of sugar maple, largetooth aspen, paper birch and balsam fir. *Tree Physiol.* **12**, 15–21.

Liu X.-M., Teng F.-Z., Rudnick R. L., McDonough W. F. and Cummings M. L. (2014) Massive magnesium depletion and isotope fractionation in weathered basalts. *Geochim. Cosmochim. Acta* **135**, 336–349.

Ma L., Teng F.-Z., Jin L., Ke S., Yang W., Gu H.-O. and Brantley S. L. (2015) Magnesium isotope fractionation during shale weathering in the Shale Hills Critical Zone Observatory: accumulation of light Mg isotopes in soils by clay mineral transformation. *Chem. Geol.* **397**, 37–50.

MacDonald J. D., Bélanger N., Sauvé S., Courchesne F. and Hendershot W. H. (2007) Collection and Characterization of Soil Solutions. In *Soil Sampling and Methods of Analysis* (eds. M. R. Carter and E. G. Gregorich), 2nd ed. CRC Press, Boca Raton, FL, pp. 179–198.

Marschner H. (1995) *Mineral Nutrition of Higher Plants*. Academic Press, London, p. 889p.

Martignole J. and Schrijver K. (1970) Tectonic setting and evolution of the Morin anorthosite, Grenville Province, Québec. *Bull. Geol. Soc. Finland* **42**, 165–209.

Mavromatis V., Prokushkin A. S., Pokrovsky O. S., Viers J. and Korets M. A. (2014) Magnesium isotopes in permafrost-dominated Central Siberian larch forest watersheds. *Geochim. Cosmochim. Acta* **147**, 76–89.

Miller E. K., Blum J. D. and Friedland A. J. (1993) Determination of soil exchangeable-cation loss and weathering rates using Sr isotopes. *Nature* **362**, 438–441.

Moore J., Jacobson A. D., Holmden C. and Craw D. (2013) Tracking the relationship between mountain uplift, silicate weathering, and long-term CO_2 consumption with Ca isotopes: Southern Alps, New Zealand. *Chem. Geol.* **341**, 110–127.

Nezat C. A., Blum J. D., Yanai R. D. and Hamburg S. P. (2007) A sequential extraction to determine the distribution of apatite in granitoid soil mineral pools with application to weathering at the Hubbard Brook Experimental Forest, NH, USA. *Appl. Geochem.* **22**, 2406–2421.

Nezat C. A., Blum J. D., Yanai R. D. and Park B. B. (2008) Mineral sources of calcium and phosphorus in soils of the northeastern United States. *Soil Sci. Soc. Am. J.* **72**, 1786–1794.

Noodén L. D., Guiamét J. J. and John I. (1997) Senescence mechanisms. *Physiol. Plant.* **101**, 746–753.

Opfergelt S., Georg R. B., Delvaux B., Cabidoche Y.-M., Burton K. W. and Halliday A. N. (2012) Mechanisms of magnesium isotope fractionation in volcanic soil weathering sequences Guadeloupe. *Earth Planet. Sci. Lett.* **341–344**, 176–185.

Opfergelt S., Burton K. W., Georg R. B., West A. J., Guicharnaud R. A., Sigfússon B., Siebert C., Gíslason S. R. and Halliday A. N. (2014) Magnesium retention on the soil exchange complex controlling Mg isotope variations in soils, soil solutions and vegetation in volcanic soils, Iceland. *Geochim. Cosmochim. Acta* **125**, 110–130.

Pessarakli M. (2016) Handbook of photosynthesis 3rd ed. CRC Press, Taylor & Francis Group, Boca Raton, FL, USA 846p.

Pogge von Strandmann P. A. E., Burton K. W., James R. H., van Calsteren P., Gislason S. R. and Sigfússion B. (2008) The influence of weathering processes on riverine magnesium isotopes in a basaltic terrain. *Earth Planet. Sci. Lett.* **276**, 187–197.

Pogge von Strandmann P. A. E., Opfergelt S., Lai Y.-J., Sigfússon B., Gislason S. R. and Burton K. W. (2012) Lithium, magnesium and silicon isotope behavior accompanying weathering in a basaltic soil and pore water profile in Iceland. *Earth Planet. Sci. Lett.* **339–340**, 11–23.

Pokharel R., Gerrits R., Schuessler J., Floor G., Gorbushina A. and von Blanckenburg F. (2017) Mg isotope fractionation during uptake by a rock-inhabiting, model microcolonial fungus Knufia petricola at acidic and neutral pH. *Environ. Sci. Technol.* **51**, 9691–9699.

Ra K. and Kitagawa H. (2007) Magnesium isotope analysis of different chlorophyll forms in marine phytoplankton using multi-collector ICP-MS. *J. Anal. At. Spectrom.* **22**, 817–821.

Ra K., Kitagawa H. and Shiraiwa Y. (2010) Mg isotopes in chlorophyll-a and coccoliths of cultured coccolithophores (*Emiliana huxleyi*) by MC-ICP-MS. *Marine Chem.* **122**, 130–137.

Riechelmann S., Buhl D., Schröder-Ritzrau A., Spötl C., Riechelmann D. F. C., Richter D. K., Kluge T., Marx T. and Immenhauser A. (2012) Hydrogeochemistry and fractionation pathways of Mg isotopes in a continental weathering system: lessons from field experiments.

Ryu J.-S., Jacobson A. D., Holmden C., Lundstrom C. and Zhang Z. (2011) The major ion, $\delta^{44/40}$Ca, $\delta^{44/42}$Ca, and $\delta^{26/24}$Mg geochemistry of granite weathering at pH = 1 and T = 25 °C: power-law processes and the relative reactivity of minerals. *Geochim. Cosmochim. Acta* **75**, 6004–6026.

Ryu J.-S., Vigier N., Decarreau A., Lee S.-L., Lee K.-S., Song H. and Petit S. (2016) Experimental investigation of Mg isotope fractionation during mineral dissolution and clay formation. *Chem. Geol.* **445**, 135–145.

Saenger C. and Wang Z. (2014) Magnesium isotope fractionation in biogenic and abiogenic carbonates: implications for paleoenvironmental proxies. *Quat. Sci. Rev.* **90**, 1–21.

Schmitt A.-D., Vigier N., Lemarchand D., Millot R., Stille P. and Chabaux F. (2012) Processes controlling the stable isotope compositions of Li, B, Mg and Ca in plants, soils and waters: a review. *C. R. Geosci.* **344**, 704–722.

Schmitt A.-D., Cobert F., Bourgeade P., Ertlen D., Labolle F., Gangloff S., Badot P.-M., Chabaux F. and Stille P. (2013) Calcium isotope fractionation during plant growth under a limited nutrient supply. *Geochim. Cosmochim. Acta* **110**, 70–83.

Smith S. E. and Read D. J. (2008) *Mycorrhizal Symbiosis*, 3rd ed. Academic Press, San Diego, USA, p. 800p.

Soil Classification Working Group (SCWG) (1998) The Canadian System of Soil Classification. Agric. and Agri-Food Can. Publ. 1646 (Revised). 187p.

Teng F.-Z. (2017) Magnesium isotope geochemistry. *Rev Mineral Geochem Mineral Soc. Am.* **82**, 219–287.

Teng F.-Z., Li W.-Y., Rudnick R. L. and Gardner R. (2010) Contrasting lithium and magnesium isotope fractionation during continental weathering. *Earth Planet. Sci. Lett.* **300**, 63–71.

Thiffault E., Paré D., Bélanger N., Munson A. and Marquis F. (2006) Harvesting intensity at clear-felling in the boreal forest. *Soil Sci. Soc. Am. J.* **70**, 691–701.

Tipper E. T., Galy A. and Bickle M. J. (2006a) Riverine evidence for a fractionated reservoir of Ca and Mg on the continents: implications for the oceanic Ca cycle. *Earth Planet. Sci. Lett.* **247**, 267–279.

Tipper E. T., Galy A., Gaillardet J., Bickle M. J., Elderfield H. and Carder E. A. (2006b) The magnesium isotope budget of the modern ocean: constraints from riverine magnesium isotope ratios. *Earth Planet. Sci. Lett.* **250**, 241–253.

Tipper E. T., Galy A. and Bickle M. J. (2008) Calcium and magnesium isotope systematics in rivers draining the Himalaya-Tibetan-Plateau region: lithological or fractionation control? *Geochim. Cosmochim. Acta* **72**, 1057–1075.

Tipper E. T., Gaillardet J., Louvat P., Capmas F. and White A. F. (2010) Mg isotope constraints on soil pore-fluid chemistry: evidence from Santa Cruz California. *Geochim. Cosmochim. Acta* **74**, 3883–3896.

Tipper E. T., Calmels D., Gaillardet J., Louvat P., Capmas F. and Dubacq B. (2012a) Positive correlation between Li and Mg isotope ratios in the river waters of the Mackenzie Basin challenges the interpretation of apparent isotopic fractionation during weathering. *Earth Planet. Sci. Lett.* **333–334**, 35–45.

Tipper E. T., Lemarchand E., Hindshaw R. S., Reynolds B. C. and Bourdon B. (2012b) Seasonal sensitivity of weathering processes: hints from magnesium isotopes in a glacial stream. *Chem. Geol.* **312–313**, 80–92.

Uhlig D., Schuessler J. A., Bouchez J., Dixon J. L. and von Blanckenburg F. (2017) Quantifying nutrient uptake as driver of rock weathering in forest ecosystems by magnesium stable isotopes. *Biogeosci.* **14**, 3111–3128.

van der Heijden G., Legout A., Mareschal L., Ranger J. and Dambrine E. (2017) Filling the gap in Ca input-output budgets in base-poor forest ecosystems: the contribution of non-crystalline phases evidenced by stable isotopic dilution. *Geochim. Cosmochim. Acta* **209**, 135–148.

Vizcayno-Soto G. and Côté B. (2004) A boundary-line approach to determine standards of nutrition for mature trees from spatial variation of growth and foliar nutrient concentrations in natural environments. *Comm. Soil Sci. Plant Anal.* **35**, 2965–2985.

Walker T. S., Bais H. P., Grotewold E. and Vivanco J. M. (2003) Root exudation and rhizosphere biology. *Plant Physiol.* **132**, 44–51.

White A. F., Bullen T. D., Davison V. V., Schulz M. S. and Clow D. W. (1999) The role of disseminated calcite in the chemical weathering of granitoid rocks. *Geochim. Cosmochim. Acta* **63**, 1939–1953.

Whittaker R. H., Bormann F. H., Likens G. E. and Siccama T. G. (1974) The Hubbard Brook Ecosystem Study: forest biomass and production. *Ecol. Monogr.* **44**, 233–252.

Wilkinson S. R., Welch R. M., Mayland H. F. and Grunes D. L. (1990) Magnesium in plants: uptake, distribution, function, and utilization by man and animals. *Met. Ions Biol. Syst.* **26**, 33–56.

Wimpenny J., Gíslason S. R., James R. H., Gannoun A., Pogge von Strandmann P. A. E. and Burton K. W. (2010) The behaviour of Li and Mg isotopes during primary phase dissolution and secondary mineral formation in basalt. *Geochim. Cosmochim. Acta* **74**, 5259–5279.

Wimpenny J., Burton K. W., James R. H., Gannoun A., Mokadem F. and Gíslason S. (2011) The behaviour of magnesium and its isotopes during glacial weathering in an ancient shield terrain in West Greenland. *Earth Planet. Sci. Lett.* **304**, 260–269.

Wimpenny J., Colla C. A., Yin Q. –Z., Rustad J. R. and Casey W. H. (2014) Investigating the behaviour of Mg isotopes during the formation of clay minerals. *Geochim. Cosmochim. Acta* **128**, 178–194.

Young E. and Galy A. (2004) The isotope geochemistry and cosmochemistry of magnesium. *Rev. Mineral. Geochem. Miner. Soc. Am.* **55**, 197–230.

Associate Editor: Andrew D. Jacobson